Swiss J Geosci (2010) 103:427–455
DOI 10.1007/s00015-010-0030-4

Potential for deep geological sequestration of CO_2 in Switzerland: a first appraisal

Gabriel Chevalier · Larryn W. Diamond · Werner Leu

Received: 10 February 2009 / Accepted: 10 August 2010 / Published online: 24 November 2010

Abstract Possibilities to sequester anthropogenic CO_2 in deep geological formations are being investigated worldwide, but the potential within Switzerland has not yet been evaluated. This study presents a first-order appraisal based solely on geological criteria collated from the literature. The Swiss Molasse Basin (SMB) and the adjacent Folded Jura are the only realms of the country where CO_2 could conceivably be stored in saline aquifers. Evaluation of geological criteria at the basin-wide scale shows that the SMB–Jura has moderate potential (score of 0.6 on a scale from 0 to 1) when compared to basins elsewhere. At the intrabasinal scale, inspection of the stratigraphy reveals four regional candidate aquifers that are sealed by suitable caprocks: top Basement plus basal Mesozoic sandstones, all sealed by the Anhydrite Group; Upper Muschelkalk sealed by the Gipskeuper; Hauptrogenstein sealed by the Effinger Member, and Upper Malm plus Lower Cretaceous sealed by the Lower Freshwater Molasse. Nine geological criteria are defined to evaluate the storage potential of these and other smaller scale candidates. A numerical scoring and weighting scheme allows the criteria to be assessed simultaneously, permitting the storage potential to be depicted using the 0–1 scale in contoured maps. Approximately 5,000 km^2 of the central SMB exhibits potentials between 0.6 and 0.96. The Fribourg–Olten–Luzern area is the most favoured owing to the presence of several sealed aquifers within the preferred 800–2,500 m depth interval, and to its low seismicity, low geothermal gradient, low fault density, and long groundwater residence times. Smaller areas with good potential lie between Zürich and St. Gallen. In contrast, western Switzerland, the Jura and the southern SMB have markedly poorer potential. Considering only the portions of the aquifers with potential above 0.6, the theoretical, effective storage capacity of the basin is estimated to be 2,680 million tonnes of CO_2.

Keywords Sequestration · Carbon dioxide · Switzerland · Swiss Molasse basin · CO_2 storage potential · Geology · Aquifer

Introduction

Carbon dioxide capture and storage (CCS) is considered to be a serious option to mitigate climate change as it has the potential to make deep cuts in the CO_2 emissions of large point sources (see IPCC 2005 for a complete review of CCS). It is an option that can be applied to the energy production sector such as coal- or gas-fired power plants, and to heavy industries such as cement factories and oil refineries.

Numerous procedures to store CO_2 in the natural environment are under investigation, such as releasing it into the deep oceans or immobilising it in mineral form via in situ carbonation reactions in basalts or ultramafic rocks. The possible side effects of the former, especially on marine biota, are poorly understood to date, and so risks are high (Harrison et al. 1995). In the latter, the sluggish carbonation rates of silicate minerals at low temperatures (shallow depths) are the main issue (Oelkers et al. 2008). A proven approach is to inject CO_2 into porous geological

Editorial handling: S. Löw & A.G. Milnes.

G. Chevalier · L. W. Diamond (✉)
Rock–Water Interaction Group, Institute of Geological Sciences, University of Bern, Baltzerstrasse 3, 3012 Bern, Switzerland
e-mail: diamond@geo.unibe.ch

W. Leu
Geoform Ltd., Via San Gottardo 56, 6648 Minusio, Switzerland

formations within sedimentary basins (e.g. Gunter and Perkins 1993; Kharaka et al. 2006; Benson and Cole 2008; Chadwick et al. 2008).

Several types of sedimentary formations have been considered. Depleted oil and gas fields are an obvious choice, because their very existence proves high capacity for fluid storage and long-term integrity of seals. Several commercial projects have demonstrated that this approach can lead to a win–win situation, as the injected CO_2 lowers the viscosity of oil and therefore improves extraction yields [a technology known as enhanced oil recovery (EOR)]. Injection of CO_2 into coal seams is thought to be another favourable scenario because CO_2 adsorbs more strongly than methane onto coal surfaces. Injected CO_2 thus displaces the natural surface-adsorbed methane, enhancing gas recovery while itself becoming fixed [a technology known as enhanced coal bed methane recovery (ECBMR)]. However, the storage capacities are generally small. In contrast, saline aquifers are widespread and voluminous, and the brines they contain are unattractive for other uses, except in some cases for geothermal energy production. Saline aquifers are being targeted as they can trap CO_2 in several ways: as a free fluid phase, as a dissolved component in the brine and eventually as stable carbonate minerals.

The envisaged CO_2-retention times are critical in selecting a suitable aquifer for storage. To counter the greenhouse effect the injected CO_2 must remain underground for at least hundreds if not thousands of years. Accordingly, the residence times of the brines, the integrity of the aquifer caprocks and the presence of structures that could either promote or prevent CO_2 leakage are of primary concern. Anticipated mechanical, hydraulic and geochemical perturbations caused by the injection of CO_2 (e.g. induced seismicity) also need to be factored into the choice of a storage site. Thus, processes such as the evolution of fluid pressure and the impact of mineral precipitation and dissolution reactions on aquifer permeability need to be predicted accurately.

The first step towards implementing CCS in deep sedimentary basins is to identify potential storage formations and their CO_2 capacities. This is not a straightforward task, because large amounts of diverse information are required to characterize subsurface conditions and to predict site-specific responses to induced perturbations. As hydrocarbon exploration is also focussed on sedimentary basins, most of the information and knowledge relevant to CCS evaluation is gained and owned by the petroleum industry. Oil- and gas-rich basins (and countries) are therefore favoured, as the required data are already at hand and only need to be processed for CCS assessment. Further, productive basins have the necessary infrastructure for rapid implementation of CO_2 storage (large industrial areas, power plants, pipelines, etc.). On the other hand, mature basins have the drawback that their numerous old exploration boreholes may act as leakage paths and thereby pose safety issues. Poorly explored basins are not well suited because the return on investment to obtain the minimum knowledge for a reliable CCS evaluation is not assured, and because infrastructure is typically not available. In spite of these complications, scientific investigations, pilot tests and commercial projects are now underway to assess and implement CO_2 storage in deep geological formations in various parts of the world (e.g. Solomon 2007; Chadwick et al. 2008; US-DOE 2008). Recently, the European Parliament launched a proposal for a directive on CCS (COM 2008), and 12 demonstration plants should be operational in Europe by 2015.

Switzerland has several point sources of industrial CO_2 emissions, including oil refineries and cement factories, which could be amenable to disposal via geological sequestration. While the country has no coal-fired power plants and they are not considered to be an option in the national energy supply perspectives (SFOE 2007), combined-cycle gas-fired power plants are under discussion as a temporary solution to cover the energy gap that will arise when the oldest nuclear power plant is decommissioned in 2020. Even in a full hydrogen-based economy, CCS would be mandatory for any large concentrated CO_2 emitters in the industrial and energy sectors.

The obvious geological basin for consideration of deep aquifer storage in Switzerland is the Swiss Molasse Basin (SMB) and the related Jura Mountains. Located to the north of the Alps, the surface of the SMB–Jura makes up 45% of the national territory and it hosts the vast majority of the population and industrial activities. The suitability of the SMB–Jura for deep CO_2 storage is somewhat equivocal at present. Petroleum exploration has so far not resulted in commercially viable prospects, with the consequence that the basin remains undeveloped and knowledge is fragmental. On the other hand, owing to increased interest in the use of the subsurface in general, several projects are currently under way to improve geological understanding of the SMB (e.g., for radioactive waste repositories, geothermal energy, water supply and underground civil engineering).

Given Switzerland's political commitment to reducing CO_2 emissions, it is now time to evaluate the options for CO_2 storage within the national boundaries. To our knowledge there are no publications on the possibilities for geological storage of CO_2 in Switzerland, except for a brief mention by Wildenborg et al. (2005) in their evaluation of the cost curve for CO_2 storage in Europe. Their study concluded that Switzerland has no potential for CO_2 storage in the foreseeable future owing to legal constraints and to the possible conflicts of use of groundwaters. However,

such objections are likely to be modified with time as policies regarding energy and the environment evolve. A detailed geological assessment on which to base future decision-making is lacking.

The present article contributes to filling this gap by evaluating the potential for deep underground storage of CO_2 within Switzerland, based exclusively on geological criteria. Information on related technological and safety issues can be found elsewhere (Holloway 1997; IPCC 2005; Benson and Surles 2006; Chadwick et al. 2008).

This article proceeds by first reviewing the principles of CO_2 storage in sedimentary formations, in order to distil a set of appropriate evaluation criteria. The literature on the geology of the SMB–Jura is then examined in the light of these criteria to identify potential storage formations. Three complementary evaluations of the SMB–Jura domain are then performed at different scales and considering different aspects of the problem: (1) a basin-wide evaluation, which treats the entire sedimentary filling of the basin as one object. This facilitates a comparison with basins elsewhere and allows the Swiss case to be set in an international context; (2) an intrabasinal evaluation, which compares the suitability of the entire sediment stack below various geographic regions. This facilities a regional appraisal of the storage potential without focussing on individual formations, and is therefore useful for regional planning; (3) another intrabasinal evaluation, which compares the suitability of example target formations within subregions of the basin. This facilitates a geologically more specific appraisal, which points the way towards selection of possible sites at a local scale. Finally, the volumes of the most promising aquifers are calculated to estimate the theoretical, effective storage capacities for CO_2. These results provide a basis to set priorities for further research and development of CO_2 storage in Switzerland.

Principles of CO_2 storage in saline aquifers

Mechanisms of CO_2 trapping in saline aquifers

Although a deep aquifer may behave as an open system on the scale of 10^4–10^6 years, several trapping mechanisms combine to retain CO_2 in the aquifer over comparable or even longer periods. Injection of CO_2 into a deep formation requires that the gas be artificially pressurized to a value greater than that of the in situ formation water (Fig. 1a). Thus, upon injection from a perforated or screened borehole, the compressed CO_2 displaces some of the formation water from the rock pores and it accumulates as an immiscible fluid plume. The post-injection density of the CO_2 fluid depends on the ambient temperature and on the pressure of the adjacent formation water. In deep aquifers with low geothermal gradients, CO_2 is stable in the supercritical fluid state with liquid-like density (Fig. 1b, c). Nevertheless, even if the P–T conditions are conducive to high density, CO_2 is still markedly less dense than any saline formation water (by a factor of 1.3–4, depending on the salinity of the brine; Fig. 1c), and it has a far lower viscosity (by a factor of 6–50, depending on salinity; Fig. 1d). These two attributes impart high buoyancy and mobility to the CO_2 plume and so it migrates away from the injection point, displacing formation water along the way.

The migration of the plume is confined to the aquifer by the low-permeability caprock (a process termed stratigraphic trapping), and it may accumulate beneath folds or beneath segments of the caprock displaced by sealing faults (a process termed structural trapping) or beneath angular unconformities or lateral lithological pinch-outs (termed stratigraphic trapping). As a non-wetting phase, a fraction of the migrating CO_2 inevitably remains locked in the rock pores along the flow path owing to the narrowness of their interconnecting throats (termed residual trapping). At the same time a fraction of the CO_2 dissolves into the formation water, the solubility being highest in low-salinity, high-pressure water in the temperature range 80–100°C (solubility falls at both higher and lower temperatures than this range). Once dissolved, the CO_2 is gradually transported away from the site of the plume by the flowing formation water (termed solubility trapping). Typical flow rates in deep aquifers are in the order of mm to cm/year, and so this mode of CO_2-trapping can be effective for very long periods. During this transport the CO_2 chemically reacts with the formation water and with the aquifer rock. In aquifers composed mostly of calcite and dolomite, the addition of aqueous CO_2 may cause dissolution of the carbonate minerals, thereby increasing the porosity of the aquifer. In sandstone aquifers the reactions may produce carbonate minerals, e.g., calcite, dolomite and siderite, which tend to clog porosity. Reaction of aqueous CO_2 with solutes in the formation water is rapid but reaction with the aquifer minerals may be very slow (e.g., Xu et al. 2004). The precipitated carbonate minerals thus fix CO_2 (termed mineral trapping), but only as long as the formation water remains enriched by the injected gas. If the aquifer is slowly recharged by CO_2-poor formation water, the carbonate minerals will gradually redissolve as the original pre-injection chemical equilibrium is re-established.

Even under the most favourable aquifer conditions the amount of CO_2 that can be dissolved in the formation water is small (e.g. $\sim 25-50\,\mathrm{kg_{CO_2}/m^3_{brine}}$; Fig. 1e; see also Bachu and Adams 2003; Portier and Rochelle 2005) and the capacity of many deep aquifers is already lowered by the natural presence of CO_2. Therefore, aquifers with large structural traps or with very large amounts of

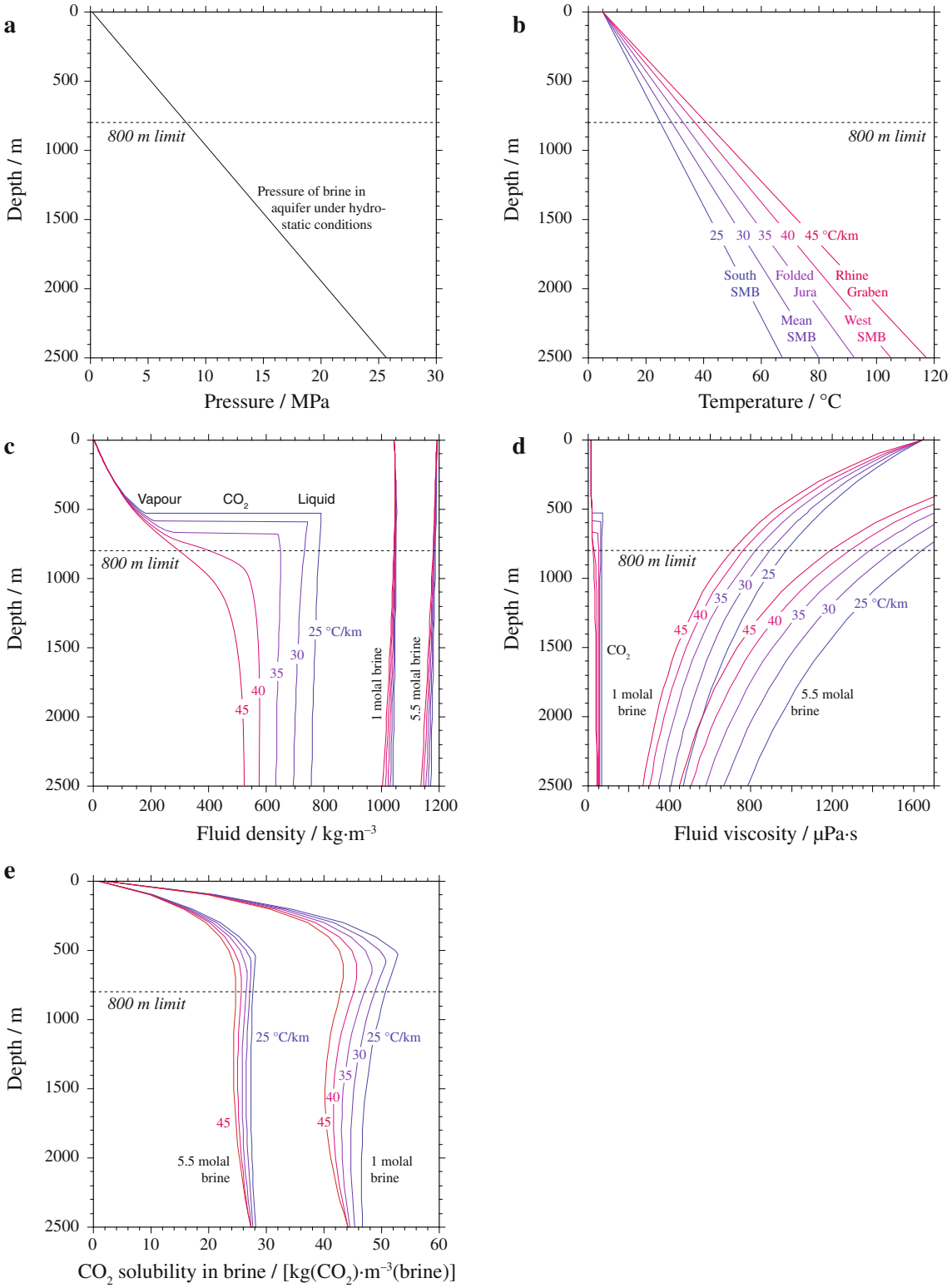

Fig. 1 Fluid properties relevant to deep geological storage of CO_2 in the Swiss Molasse Basin (SMB), plotted as a function of depth. *Dashed line* at 800 m marks the minimum depth recommended for CO_2 injection. Two examples of brines are shown: *low salinity* 1 molal NaCl (5.5 mass% NaCl) and *high salinity* 5.5 molal NaCl (24.3 mass% NaCl), from data in Mao and Duan (2009) and Akinfiev and Diamond (2010). Data for pure CO_2 from Span and Wagner (1996). **a** Pressure of in situ formation brine assuming hydrostatic conditions. **b** Range of geothermal gradients in the SMB (Rybach 1992). **c** Comparison of fluid densities for CO_2 and CO_2-saturated brines over the range of geothermal gradients in the SMB. **d** Comparison of fluid viscosities for the range of geothermal gradients in the SMB. **e** Solubility of CO_2 in model NaCl brines

formation water must be found to dispose of significant quantities of waste CO_2. Tightly sealed structural traps are the preferred sites because storage is permanent. In the absence of structural traps, CO_2 dissolved in the aquifer water may eventually degas when the water discharges into higher-level formations or even to the Earth's surface. In this case the period over which CO_2 is retained underground is finite. Nevertheless, water residence times in the order of several thousand years are common and these are thought to be sufficient to mitigate global warming until future technologies solve the problem permanently (Lindeberg and Bergmo 2002; Hepple and Benson 2005; IPCC 2005).

Geological requirements of a storage site

The geological requirements of a suitable storage site are dictated by the constraints of the injection procedure and of the CO_2 trapping mechanisms outlined above. Thus, similar to targets for hydrocarbon accumulations, a target site for CO_2 storage must consist of an aquifer–seal pair: a thick reservoir rock with sufficient permeability to permit rapid injection and sufficient porosity for high storage capacity, overlain by an extensive, low-permeability caprock. The formation water must be saline and slow-moving, and the site must be distant from its ultimate discharge zone. The aquifer must be deep enough to ensure that the injected CO_2 is highly compressed by the formation water, thereby maximising storage capacity. Suitable CO_2 densities are reached at depths >800 m, depending mainly on the geothermal gradient of the basin (Bachu 2003; Fig. 1). Drilling and CO_2 compression costs limit the maximum injection depth to around 2,500 m. A simple structural setting is preferred, so as to limit the scope for unpredictable escape conduits for CO_2. Active and permeable fault zones must be avoided to minimise the risk of leakage, as must seismic zones in general.

Once a potential aquifer has been located, the flow regime of the formation water needs to be characterized prior to injection and the possibility of induced perturbations to this regime need to be evaluated. As CO_2 injection will raise the fluid pressure in the aquifer, the capillary entry pressure of the caprock has to be tested, and the existing state of stress needs to be known to judge the risk of induced seismicity. Because injected CO_2 will react with the existing rock–water system, pre-injection geochemical states have to be measured or estimated in order to predict and then monitor the post-injection geochemical evolution with time. This requires knowledge of the three-dimensional geometry and extent of the target site, the physical rock properties of both reservoir and seal, and their mineralogy and in situ fluid compositions.

Evaluating a basin in terms of the above requirements is only possible if a good deal of information is available about the subsurface. It follows that the chances of delineating a potential site are highest where the density of information is highest. Accordingly, the state of knowledge of the subsurface, commonly referred to as "exploration maturity" in the petroleum industry, can be used as an additional criterion to screen the basin of interest for its potential for CO_2 storage.

Screening of major geological zones in Switzerland

The first step in evaluating the potential for CO_2 storage in Switzerland is to identify large-scale geological zones that may warrant more detailed examination. The geology of Switzerland comprises three main zones (Fig. 2): the Alps, the Swiss Molasse Basin (SMB) and the Jura domain (Trümpy 1980). The Alps are not considered to present significant CO_2 storage potential for several reasons. The rocks are dominantly metamorphic with low matrix porosities and permeabilities, their locally intense fracture-porosity is unconfined, and they are characterised by complicated structures. The glacially over-deepened alpine valleys contain at most several hundred meters of sediments and so they are too shallow to offer any major potential. By contrast, the sedimentary fill of the Swiss Molasse Basin (SMB) is spatially extensive and up to 6,000 m deep. It therefore has the largest potential for CO_2 storage in Switzerland. The Jura domain can also be considered for CO_2 storage, even though it is not a sedimentary basin, as it includes most of the formations found in the SMB.

For the above reasons the remainder of this evaluation deals exclusively with the SMB and the adjacent Jura domain. Figure 2a and b show cross-sections through these two zones, with the most favourable depth interval for CO_2 injection (800–2,500 m) marked by dashed lines. Prior to proceeding with the evaluation of the storage potential of these zones, the necessary background information on the geological history and current tectonic setting of the basin is summarized.

Geological overview of the SMB and adjacent Jura

The SMB belongs to a major regional depression known as the North Alpine Foreland Basin, the remnant of a synorogenic downwarp extending from Savoy (France) to Linz (Austria). The SMB occupies the western and central part of the Foreland Basin, stretching over approximately 300 km between Savoy in the SW and Lake Constance in the NE. Along its length the SMB widens towards the NE from about 30 km near Geneva to 80 km at Lake Constance (Fig. 2).

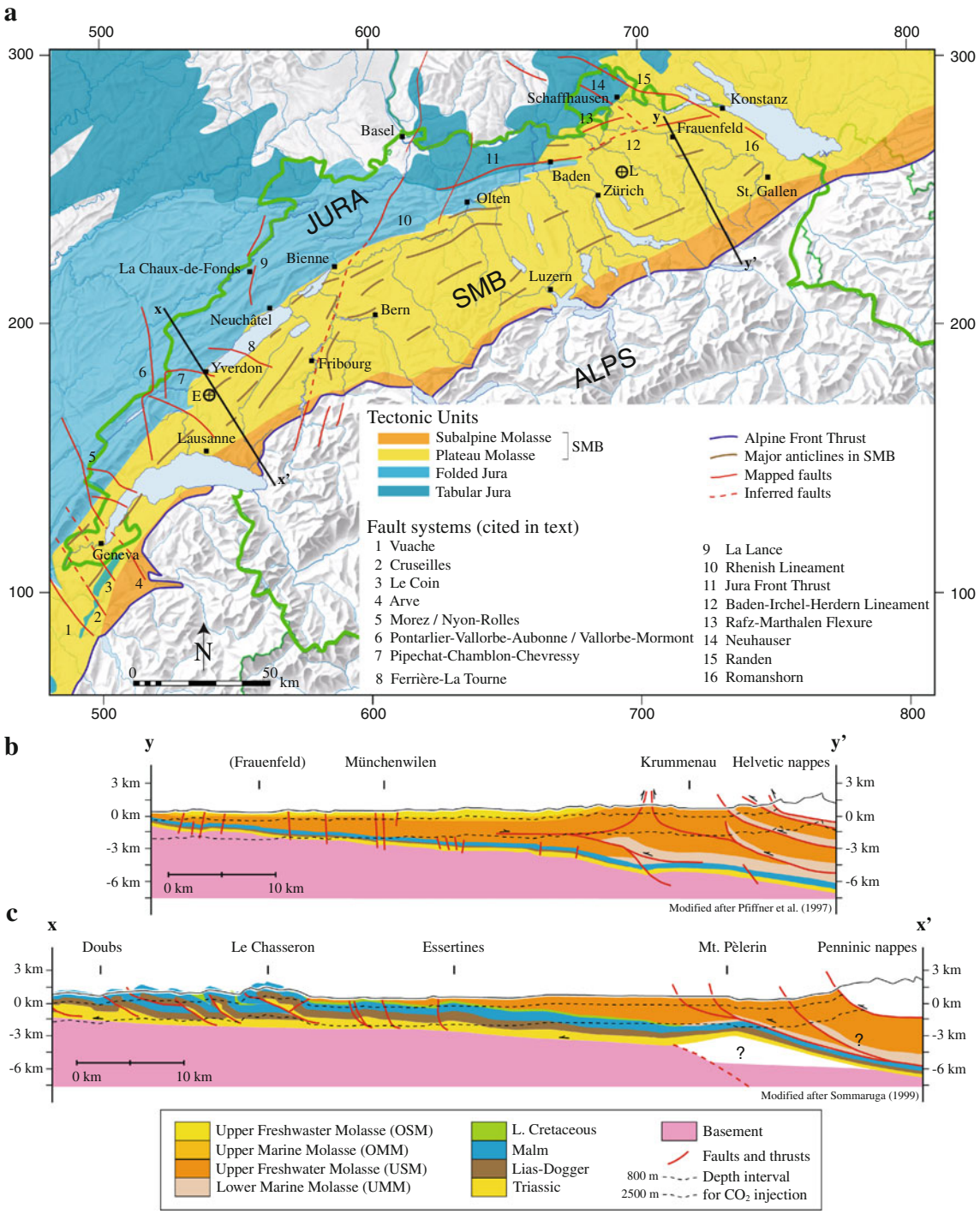

Fig. 2 Geology of the Swiss Molasse Basin (SMB). **a** Map with structures and localities mentioned in text. *Thick green line* is the national border. *Coordinates* are Swiss km grid. **b** Cross-section *y*–*y*′ after Pfiffner et al. (1997). **c** Cross-section *x*–*x*′ after Sommaruga (1999)

Geological history of the North Alpine Foreland Basin

More than 300 Ma of Earth's history is responsible for all the elements in the current makeup of the SMB. The geological evolution is ascribed to four tectonic phases (e.g. Mazurek et al. 2006): (1) a period of transpressive strike-slip tectonics in the Permo-Carboniferous, which formed wrench troughs in the crystalline Variscan basement that became filled by up to several thousand meters of clastic sediments; (2) shallow-marine sedimentation in an epicontinental sea throughout most of the Mesozoic, resulting in a 1,000–2,000 m thickness of minor sandstones

overlain by alternating evaporites, limestones, marls and shales. This sedimentation was followed by a first phase of basin inversion and of erosion down to the Upper Jurassic units; (3) development of a foreland basin as a consequence of the Early Eocene collision between the European and Adria plates, with deposition of syn-orogenic conglomerates, sandstones and shales (more than 4,000 m thick in the SE, diminishing to a few hundred meters thickness in distal portions towards the NE); (4) a second phase of basin inversion with attendant deformation, uplift and erosion, which commenced in the Late Miocene. This exhumation was much more pronounced in the SW, where more than 2,000 m of Cenozoic sediments were eroded, in contrast to about 1,000 m in the NE (Schegg and Leu 1998; Mazurek et al. 2006). Along its continuation towards the NE into Germany, the basin has remained mostly in an extensional regime (Brink et al. 1992). Today the SMB has the form of a wedge dipping about 4° towards the Alps, the stack of Mesozoic–Cenozoic strata reaching a depth of more than 6,000 m at the Alpine Front (Trümpy 1980; Pfiffner et al. 1997).

Tectonic setting of the SMB–Jura

Four main tectonic units are differentiated north of the Alpine border: the Subalpine Molasse, the Plateau Molasse, the Folded Jura and the Tabular Jura (Fig. 2). The first two belong to the Swiss Molasse Basin proper, while the Folded and Tabular Jura represent the Jura domain (referred to simply as the "Jura" hereafter).

Subalpine Molasse

In outcrop the Subalpine Molasse is a 10–20 km wide strip running along the northern rim of the Alpine Front (Fig. 2a). It is made up of a series of steeply inclined thrust sheets of Tertiary sediments that flatten out at depth along a basal detachment horizon (Trümpy 1980; Fig. 2b, c), which developed during the Middle or Late Miocene. This complex is in turn overridden by a stack of Helvetic and Penninic Alpine nappes. A structural transition is visible at the border between the Subalpine Molasse and the Plateau Molasse: in eastern Switzerland it takes the form of a triangle zone with backthrusts and complex duplex cores (Fig. 2b); in central Switzerland the transition is dominated by steep backthrusts and folds; whereas west of the Aare valley the Subalpine Molasse overrides the Plateau Molasse (Fig. 2c). Little information is available on the stack of Mesozoic sediments underlying the Subalpine Molasse. In the east of the basin the Mesozoic units were probably not involved in the thrusting, but they may have been implicated in the west (Gorin et al. 1993). Even less information exists about the Paleozoic basement beneath the Subalpine Molasse.

Plateau Molasse

This unit represents the largest part of the SMB (Fig. 2a). The stack of Mesozoic–Tertiary sediments is considered to be autochthonous at the eastern border, whereas signs of increasing deformation appear towards the SW. Deformed fossils, pressure-solution of pebbles and higher seismic velocities than those of the corresponding formations in Bavaria indicate more intensive deformation (Lohr 1967; Trümpy 1980; Schrader 1988). Moving to the SW, large anticlinal and synclinal flexures appear at the surface. In the central and western regions the entire stack of sediments was detached along the Triassic evaporites and displaced to the NW during the Middle to Upper Miocene thin-skinned Alpine shortening known as the "Fernschub" or "Distant Push" (Laubscher 1961).

Folded Jura

The Folded Jura is a fold and thrust belt that developed during the Fernschub tectonics. Its main detachment horizon is situated in the Triassic evaporites (e.g. Fig. 2c). The belt stretches from Chambéry, situated far to the SW in France, sweeping NW of Geneva through an arc of almost 90° to reach the area of Baden in the NE (Fig. 2a). Thick, competent layers of Mesozoic limestones define the fold structures, while less competent sediments have often acted as secondary detachments, becoming tectonically thickened in the cores of the anticlines. Relicts of Tertiary sediments occur in small packets within the larger synclines. The belt narrows markedly at Olten, the last anticline dying out just east of Baden.

Tabular Jura

The Tabular Jura represents the autochthonous Mesozoic cover in NE Switzerland and the Ajoie area. The strata dip slightly towards the south, where they become buried under the Tertiary sediments of the Plateau Molasse (Fig. 2a). The name Tabular originates from the typical geomorphology of this region, which consists of elevated plateaus dissected by a grid of faults and valleys. To the north of the Tabular Jura older units crop out, reaching down to the Triassic (for instance in the Wutach valley).

Lithostratigraphy of the SMB–Jura

In Fig. 3 the lithologies that make up the SMB and adjacent Jura have been compiled into a synthetic, two-dimensional column, based on eight profiles assembled by

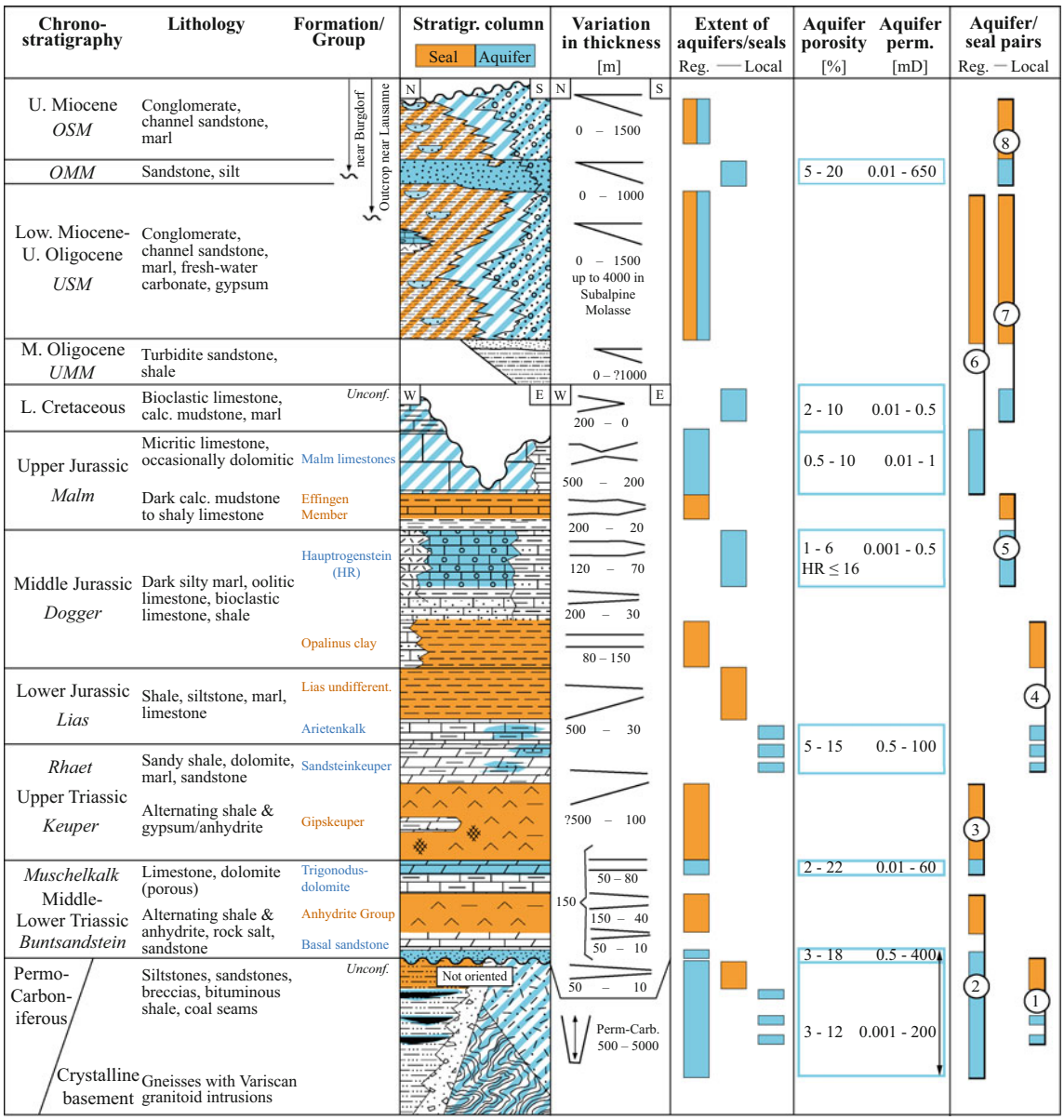

Fig. 3 Generalized stratigraphic column (not to scale) of the Swiss Molasse Basin and the adjacent Folded Jura, showing aquifer properties relevant to the geological storage of CO_2. Aquifers are *blue*, aquitards *orange*. The *rightmost column* shows the eight main aquifer/seal pairs described in "Parameterization of the geological evaluation criteria" of the text. Stratigraphy based on Jordan (2007). Aquifer properties from Schegg et al. (1997) and from unpublished borehole data (SEAG, Swissgas)

Jordan (2007; profiles 1–8). Additional data were obtained from Büchi et al. (1965); Nagra (1985, 1988, 1989, 1990, 1991); Matter et al. (1988); Peters et al. (1989); Keller (1992); Gorin et al. (1993); Jenny et al. (1995); Schegg et al. (1997, 1999), and Naef (2006). The stratigraphic column shows only the largest facies changes on a regional scale. The lateral variation in thickness of the formations is displayed schematically by divergent lines in the adjacent column in Fig. 3. The Tertiary sediments mostly exhibit facies variations along a N–S axis, whereas the Mesozoic sequence shows the greatest variations parallel to the E–W axis of the basin. This is well demonstrated by comparing the stratigraphic thicknesses in two drillholes at Essertines in the SW and Lindau in the NE of the SMB (Fig. 4; locations marked E and L in Fig. 2a). At Essertines the Mesozoic is over 2.6 km thick but it reduces to only 800 m at Lindau. Therefore, the orientation of the stratigraphic column in Fig. 3 is switched from N–S to W–E below the Middle Oligocene. As the pre-Triassic units are not known to have simple or monotonic geographical variations, no compass orientation is assigned to the column below the basal unconformity.

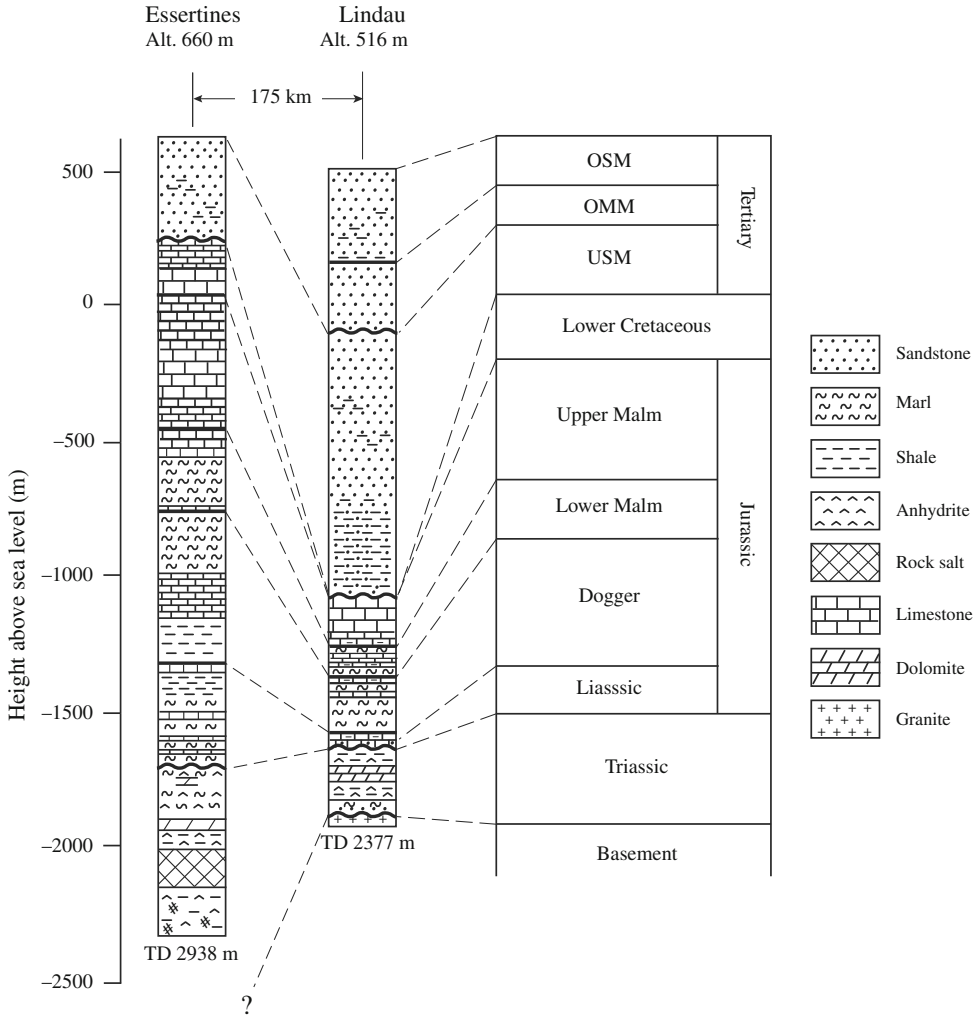

Fig. 4 Stratigraphic columns at Essertines and Lindau (locations marked in Fig. 2a by *encircled crosses* labelled *E* and *L*, respectively), illustrating sequences and variations in thicknesses of strata in the Plateau Molasse. The two sites are 175 km apart. Modified after Sommaruga (1997) and Büchi et al. (1965). *OSM* Upper Freshwater Molasse, *OMM* Upper Marine Molasse, *USM* Lower Freshwater Molasse

Methodology for quantitative evaluation of CO_2 storage potential

Having identified the main geological zones of interest for CO_2 storage, the next step is to adopt a methodology that permits their meaningful evaluation. It would be preferable to take an objective, quantitative approach, which can be applied at different spatial scales. However, this is not feasible with the current state of knowledge of the SMB–Jura. Drillhole data are generally too sparse to provide reliable quantification of some of the key parameters, and so both the screening and weighting of geological information require subjective decision-making. Consequently, we have adopted the qualitative screening and ranking methodology proposed by Bachu (2003) to evaluate the CO_2 storage potential of entire sedimentary basins. This will be applied without modification to our evaluation of the SMB–Jura at the basin-wide scale. The same overall approach is applied to our second and third evaluations, each of which is conducted at the intrabasinal scale, but the choice and weighting of criteria will be modified to suit the changes in purpose and scale, as explained below.

Methodology for basin-wide evaluation

The principle of the Bachu (2003) approach is as follows. A set of basin-scale criteria is defined, as shown in Table 1, and for each criterion several classes are distinguished. Based on geological experience largely from the petroleum industry, the relative suitability of the classes for CO_2 storage is described by a simple, monotonically increasing numerical function. Thus, each class is assigned a numerical value, or "score". For example, criterion 6 in Table 1 concerns the geothermal gradient. "Warm", "moderate" and "cold" are the corresponding classes. Because CO_2 injected into a cold basin is denser and more soluble in formation water than in a warm basin (Fig. 1), the storage capacity of the available porosity in a cold basin will be higher. Accordingly, warm basins (>40°C/km) receive a score of 1 whereas cold basins (<30°C/km) receive a score of 7.

Table 1 Criteria and their weights used in evaluating the potential of sedimentary basins for geological storage of CO_2, following the methodology of Bachu (2003)

Criterion		Classes (and relative scores in square brackets)					Weight
		A	B	C	D	E	
1	Tectonic setting	Convergent oceanic (episutural) [1]	Convergent intramontane (episutural) [3]	Divergent continental shelf [7]	Foredeep (perisutural) [15]	Cratonic [15]	0.07
2	Size	*Small [1]*	Medium [3]	Large [5]	Giant [9]		0.06
3	Depth	Shallow (<1,500 m) [1]	*Intermediate (1,500–3,500 m) [3]*	Deep (>3,500 m) [5]			0.07
4	Geology	Extensively faulted and fractured [1]	*Moderately faulted and fractured [3]*	Limited faulting and fracturing, extensive shales [7]			0.08
5	Hydrogeology	Shallow, short flow systems or compaction flow [1]	*Intermediate flow systems [3]*	Regional, long-range flow systems; topography or erosional flow [7]			0.08
6	Geothermal	Warm basin [1]	Moderate [3]	*Cold basin [7]*			0.10
7	Hydrocarbon potential	None [1]	*Small [3]*	Medium [7]	Large [13]	Giant [21]	0.06
8	Exploration maturity	Unexplored [1]	Exploration [2]	*Developing [4]*	Mature [8]	Overmature [10]	0.08
9	Coals and CBM	None [1]	*Deep (>800 m) [2]*	Shallow (200–800 m) [5]			0.04
10	Salts	None [1]	Domes [2]	*Beds [3]*			0.01
11	On/offshore	Deep offshore [1]	Shallow offshore [4]	*Onshore [10]*			0.10
12	Climate	Arctic [1]	Sub-Arctic [2]	Desert [4]	Tropical [7]	*Temperate [11]*	0.08
13	Accessibility	Inaccessible [1]	Difficult [3]	Acceptable [6]	*Easy [10]*		0.03
14	Infrastructure	None [1]	Minor [3]	*Moderate [7]*	Extensive [10]		0.05
15	CO_2 Sources	None [1]	*Few [3]*	Moderate [7]	Major [15]		0.09

The Swiss Molasse Basin corresponds to the *italicized classes*

The various criteria have different impacts on overall storage potential and so they are assigned different weights (last column in Table 1). For example, the geothermal state of the basin is weighted 0.1, whereas the presence of salt deposits (in which CO_2 could conceivably be stored in excavated caverns) is weighted only 0.01. Evidently, Bachu (2003) considers the geothermal characteristics of the basin to be ten times more important for CO_2 storage potential than the presence of salt deposits. Finally, the weighted scores from all the criteria are summed to yield the nominal storage potential of a given basin, the results being normalized such that a basin with excellent potential would score 1.0.

Applying this methodology to Canada, Bachu (2003) found that the 12 major sedimentary basins vary considerably in their potential. For example, the St. Lawrence and Alberta basins score 0.31 and 0.96, respectively.

Methodology for intrabasinal evaluation

None of the classified criteria listed in Table 1 can be meaningfully applied to a purely geological evaluation at the intrabasinal scale. The subset of criteria that concern geological characteristics are too general and their classes too broad. Criteria that are valid at a more local scale are presented by Chadwick et al. (2008), based on the collective experience of five CO_2 injection projects in Europe. Chadwick et al. (2008) assigned these criteria quantitative limits (Table 2) to distinguish favourable ("positive") from marginal ("cautionary") values.

While Table 2 serves as an ultimate guide for the Swiss case, for various reasons not all its criteria can be applied yet to screen the lithostratigraphy of the SMB–Jura. First, the criterion of total storage capacity presupposes knowledge of the mass of CO_2 that will need to be sequestered.

Table 2 Key geological indicators for storage-site suitability (Chadwick et al., 2008)

Storage capacity	Positive indicators	Cautionary indicators
Total storage capacity	Total capacity of reservoir estimated to be much larger than the total amount produced from the CO_2 source	Total capacity of reservoir estimated to be similar to or less than the total amount produced from the CO_2 source
Reservoir properties		
Depth (pressure)	1,000–2,500 m	<800 m or >2,500 m
Thickness (net)	>50 m	<20 m
Porosity	>20%	<10%
Permeability	>300 mD	<10–100 mD
Salinity	>100 g L^{-1}	<30 g L^{-1}
Caprock properties		
Lateral continuity	Unfaulted	Laterally variable, faults
Thickness	>100 m	<20 m
Capillary entry pressure	Much greater than buoyancy force of maximum predicted CO_2 column height	Similar to buoyancy force of maximum predicted CO_2 column height

This quantity has still not been officially stated for Switzerland, and so we choose to use the lateral extent of potential reservoir rocks as a selection criterion, the idea being that aquifers of regional extent are the most interesting because they offer the largest storage capacities. Accordingly, we evaluate the known aquifers in terms of three spatial categories: regional (>2,500 km^2), subregional (400–2,500 km^2) and local (<400 km^2).

Second, the quantitative porosity and permeability data listed in Fig. 3 and the salinity and capillary entry pressures in the literature are too sparse and their ranges too large to derive reasonably accurate representative values for the SMB–Jura. The data originate mostly from boreholes situated in the NE of the SMB; few data are available for the western and southern regions. We have therefore decided not to use numerical values of these parameters as screening criteria for individual formations at this stage. As a proxy, we rely on the qualitative values implicit in the well known aquifer or sealing characteristics of the various formations: these are the units that in the literature are considered to be "good aquifers" or "good sealing units", based on a variety of observations. The lithological sequence of the SMB–Jura has already been screened with respect to these hydrogeologic properties by Nagra, the Swiss National Cooperative for the Disposal of Radioactive Waste (Nagra 1988) and by the geothermal exploration community (Beaujard et al. 2006; Signorelli and Kohl 2006; Beaujard et al. 2007). Thus, these works serve as a valuable basis for the present study.

Chadwick et al. (2008) do not provide quantitative limits on other criteria such as seismicity, fault density and hydrogeology. However, from their guidelines and from the list of requirements of storage sites given in "Principles of CO_2 storage in saline aquifers" above, it is obvious which criteria need to be included in an intrabasinal evaluation. Our hybrid list of nine criteria is given in Table 3. Our choices of weights, classes and scores integrate the recommendations of Bachu (2003) and Chadwick et al. (2008), and these choices are justified further below.

Geological screening of the SMB–Jura at the intrabasinal scale

The following intrabasinal screening consists of three parts: (1) examination of the lithologic sequence in the basin to identify suitable aquifer and seal formations; (2) definition of classes for the nine criteria in Table 3, based on a discussion of the regional geology of the SMB–Jura; (3) assignment of scores for the classes and weighting factors for the criteria.

Identification and description of target formations

In Fig. 3 the well known aquifers are coloured in blue, and seals in orange. Moderate or heterogeneous aquifers and seals are represented by striped colours. Uncoloured formations are those with unfavourable properties (e.g. high lithologic heterogeneity, intermediate permeabilities between aquifers and seals) and are not considered further.

Eight aquifer/seal pairs have been identified as potentially interesting for CO_2 sequestration (numbered 1–8 in the rightmost column in Fig. 3). The pairs differ significantly in their lateral extent, and only three are considered to be regionally extensive. In the following the aquifer/aquiclude properties of the five pairs with subregional or local extents are described first in brief, then the properties of the three nominally more promising regional pairs are

Table 3 Criteria, scores and weights used to rank the CO_2 storage potential of regions within the SMB and adjacent Jura

Criterion		Classes [and relative scores in square brackets]				Weight
		A	B	C	D	
For evaluation of entire sediment stack at depth ≥800 m						
1a	Depth to sealed[a] aquifers	>2,500 m [1]	800–2,500 m [15]			0.20
For evaluation of individual aquifers within 800–2,500 m depth interval						
1b	Thickness of sealed[a] aquifer	≤20 m [1]	Maximum thickness of formation [15]			0.20
2	Geothermal gradient	>35°C/km [1]	30–35°C/km [8]	<30°C/km [15]		0.15
3	Hydrogeology	High complexity, poor knowledge [1]	Regional discharge zones [5]	Infiltration and transit zones [15]		0.15
4	Exploration maturity	Unexplored [1]	Moderate [11]	High [15]		0.15
5	Seismicity	Elevated [1]	Moderate [5]	Low [15]		0.10
6	Fault systems	High density/active/favours leakage [1]	Buried/favours traps [8]	Limited faulting [15]		0.10
7	Structural traps	Open-dipping structures [1]	Tilted faults, compartments [9]	Duplex structures [13]	Anticlinal structures [15]	0.10
8	Stress regime	Strike-slip to thrust faulting [1]	Strike-slip to normal faulting [15]			0.05

[a] Sealed when low-permeability caprock ≥20 m thick

presented in detail. As injection of CO_2 at depths shallower than 800 m is not recommended, the focus is on the portions of the aquifers that lie at greater depths and that are sealed by a layer of appropriate caprock at least 20 m thick.

Subregional to local-scale pairs of target formations

Permo-Carboniferous troughs (No. 1 in Fig. 3) Deep troughs under the SMB were first discovered during a drilling and seismic campaign by Nagra (e.g. Diebold et al. 1991). The intersected Konstanz–Frick trough is about 10–20 km wide and more than 100 km long, running ENE–WSW from the northern end of Lake Constance under the Tabular Jura to the Ajoie district. Along its long axis the trough varies in depth from 600 m to over 5,000 m. Other hidden Permo-Carboniferous troughs are indicated by seismic data near Olten, Bienne and the Geneva area, but with poorly known dimensions and depths (Brink et al. 1992; Gorin et al. 1993). Further troughs are located under the Subalpine Molasse, as proven by the gas production well Entlebuch-1 (Vollmayr and Wendt 1987), in Canton Lucerne. Most recently, Sommaruga and Eichenberger (2010) have extended the seismic interpretations, identifying some 18 troughs of various sizes distributed throughout the SMB. The Permian lithologic sequence within the troughs contains sandstones with potential reservoir properties and they are sealed above by playa mudstones or by oxidized shales and siltstones. The Carboniferous also contains sandstones but their permeabilities are probably too low to present any potential. However, the Carboniferous also contains small coal beds which, owing to their considerable depth, may have some potential for ECBM as a niche application for CO_2 storage in Switzerland.

Sandsteinkeuper, Arietenkalk/Opalinus Clay (No. 4 in Fig. 3) The Upper Triassic Sandsteinkeuper (comprising the Stubensandstein, Schilf Sandstone and Gansiger Dolomit; in total up to 20 m thick) and the Lower Jurassic Arietenkalk (a few m thick) may all have potential for local, small-scale storage mainly in the NE of the basin. The intervening, laterally variable marls within these formations are possible sealing units. The Lower Jurassic mudstones constitute an extensive caprock, which is up to 500 m thick in the west. Finally, the overlying Opalinus Clay of the Middle Jurassic provides another regional-scale seal with optimal properties (Nagra 2002).

Hauptrogenstein/Effingen Member (No. 5 in Fig. 3) This Middle Jurassic oolitic limestone is a potential reservoir for the central part of the SMB. In the triangular area Yverdon–Entlebuch–Aarau its lies within the 800–2,500 m depth range with thicknesses between approximately 20 and 180 m (Fig. 5a). Within the SMB there is very limited knowledge of its aquifer properties, but it appears that the formation water is brackish (e.g. 2–4 g/L TDS in the Hermrigen-1 borehole). In contrast, the Hauptrogenstein is known to be an excellent groundwater resource in the Folded Jura (Neuchâtel, La Chaux-de-Fonds). The

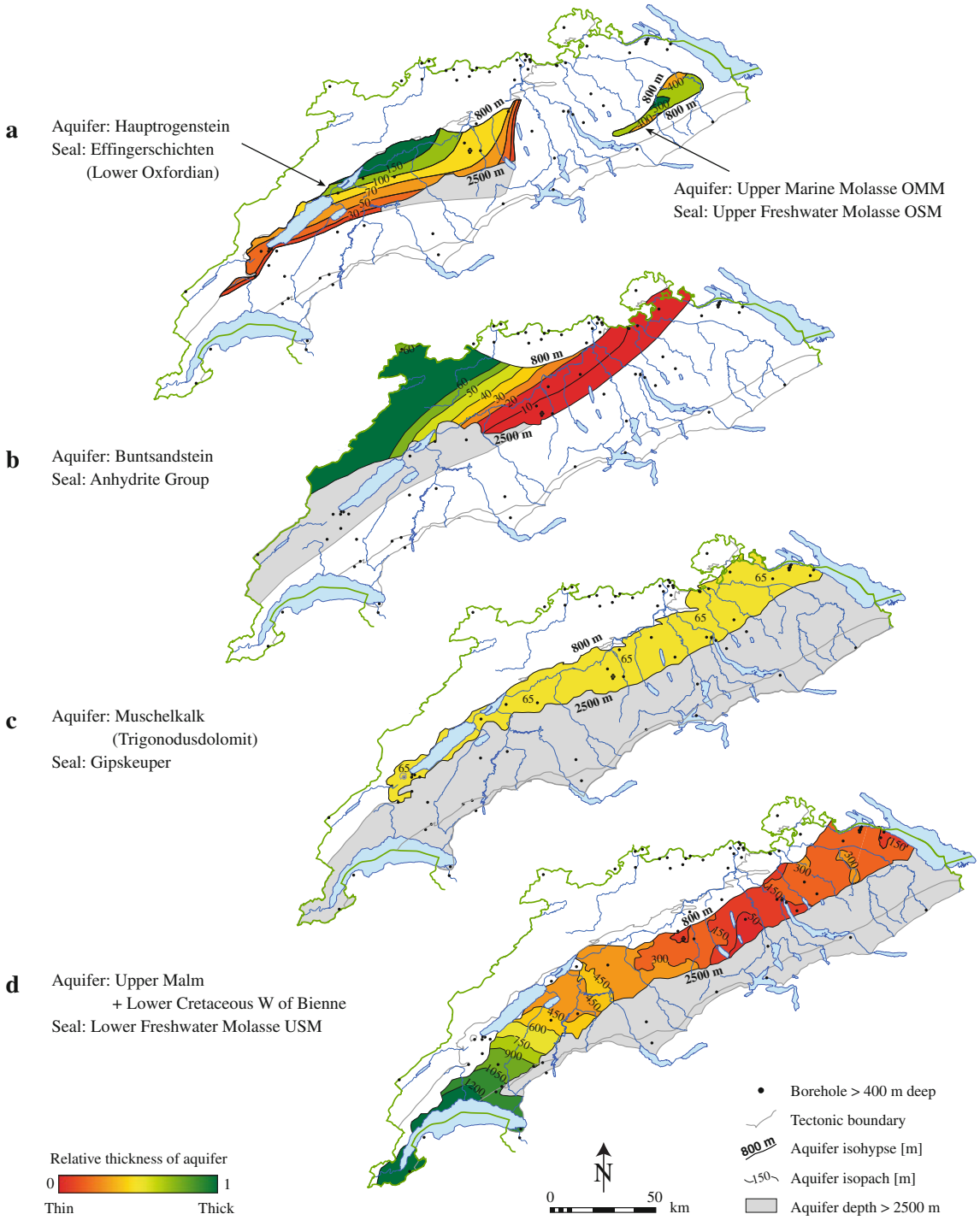

Fig. 5 Geographical extent of five major aquifers in the Swiss Molasse Basin and adjacent Jura at depths >800 m. All the aquifers are sealed by low-permeability caprock >20 m thick. *Black contours* *vertical thicknesses* (m). *Colours*: variation in *thickness* within each aquifer between minimum (*red*) and maximum (*green*). *Thicknesses* can be compared between aquifers; *colours* cannot be compared. *Grey* portions of aquifers deeper than 2500 m (thickness not contoured)

overlying Effingen Member of the Upper Jurassic, which consists of marls and shaly limestones, is a promising sealing unit.

Lower Cretaceous/Lower Freshwater Molasse USM (No. 7 in Fig. 3) The Cretaceous is entirely missing in the eastern half of the basin (e.g. Fig. 4), either because it was never

deposited or because it was eroded. However, west of the line Fribourg–Bienne a succession of neritic carbonates occurs containing marly intercalations (Gwinner 1971). The thickness increases to the SW along the axis of the basin, reaching about 300 m at Geneva. Towards the south, younger Cretaceous units are preserved up to the Cenomanian. The porosity is heterogeneous, being dominated by karst features. Whereas the aquifer properties of the Pierre Jaune de Neuchâtel (Hauterivien) are well known in the Folded Jura, better characterisation is needed elsewhere. In the SMB it is likely that the Lower Cretaceous acts as a combined aquifer with the underlying Upper Malm. The two aquifers have therefore been combined in Fig. 5. The Lower Freshwater Molasse (USM in Fig. 3) is the next large potential sealing unit moving up through the column.

Upper Marine Molasse OMM/Upper Freshwater Molasse OSM (No. 8 in Fig. 3) The Upper Marine Molasse (denoted OMM in Fig. 3) was deposited under shallow marine conditions during the Middle Miocene. Sandstones are the dominant lithology (Formations of St-Gallen and Lucerne) followed by conglomerates and minor mudstones. Only a relatively small, synformal sliver of the OMM lies deeper than 800 m (Fig. 5a). It stretches over 50 km between Lake Zürich and St. Gallen and reaches a thickness of just over 500 m. The porosity of the sandstones within the OMM varies from 5 to 20%, and the whole unit can be regarded as a regional aquifer with good horizontal permeability (up to several hundred mD) and lower vertical permeability due to thinning-upwards cycles. No direct data are available for the sliver shown in Fig. 5a, but the nearest boreholes, which lie to the east of Zürich, show transmissivities between 10^{-5} and 10^{-7} m^2 s^{-1}.

The overlying Upper Freshwater Molasse (OSM), of Upper Miocene age, represents the potential sealing unit. The general area of the OMM sliver in Fig. 5a lies on the northern margin of the Hörnli alluvial megafan (Nagra 2008). Here the OSM consists of conglomerates in the south, grading into sandstones and mudstones in the north. The sandstones and conglomerates act as local aquifers trapped in a low permeability, finer-grained matrix. However, the abundance of mudstones and their precise sealing capacity are not known. As mentioned above, the area is devoid of deep boreholes and so predictions are based on extrapolations of facies relationships. Nevertheless, owing to the large vertical variations in the lithologies, the vertical permeability in the OSM is considered to be low in most regions (Nagra 2008).

Regional-scale pairs of target formations

Buntsandstein and crystalline basement/Anhydrite Group (No. 2 in Fig. 3) The Mesozoic sequence commonly begins with sandstones of Lower Triassic (Buntsandstein) or Middle Triassic ages. Most of the Buntsandstein is a quartz-rich sandstone that is variably cemented by calcite and clays. It is known to be present in the NE of the basin, north of the approximate line Olten–Schaffhausen–Constance (Büchi et al. 1965; Gwinner 1971; Ramseyer 1987). Its extension to the SW is poorly known, but if present it probably lies north of the line Olten–Bern–Lausanne. Its thickness is around 10–20 m, increasing northwards and decreasing to the south and SE. Mean values of porosity and permeability are around 10% and 200 mD, respectively, but the spread in values is high, depending on the local degree of pore-clogging by cement minerals.

The Middle Triassic sandstone is coarse and quartz-rich. It is often called the Basal Sandstone (Basissand) and is probably equivalent to the Melser sandstone. It presumably covers most of the basin, except for the NE, where it becomes dolomitic and argillaceous (Wellendolomit, part of the Wellengebirge Formation; Gwinner 1971). It is mostly around 10 m thick with local variations up to approximately 60 m. The sandstone has variable porosity and permeability, depending on the degree of cementation and clay content. The values are probably comparable to those of the Buntsandstein.

For the sake of simplicity, we combine the two sandstones in the following discussion and use the term Buntsandstein collectively for both. To the NW in the Folded Jura this combined unit is up to 60 m thick but it thins towards the SE, reaching the critical limit of 20 m (Table 2) along the northern margin of the SMB (Fig. 5b). Further east it pinches out completely within the 800–2,500 m depth interval, but in the SW it persists below 2,500 m.

The underlying crystalline basement is composed of Paleozoic granites and gneisses. It has been extensively studied by Nagra in the NE of the basin (Mazurek and Peters 1992; Thury et al. 1994), whereas it remains mostly unknown elsewhere. In Switzerland the basement is entirely covered by Mesozoic and Tertiary sediments, except locally around Laufenburg. From the Nagra studies (Thury et al. 1994) it appears that the upper 500 m of the basement can have locally much higher hydraulic conductivity ($K \sim 10^{-7}$ m/s) than the deeper rocks ($K \sim 10^{-10}$ m/s). Drillcores show that the water-conducting zones are lithological and structural discontinuities: cataclastic zones, fracture zones with open joints, and aplites and aplitic gneisses that have focussed brittle deformation. The permeable zones are discrete, 1–100 m wide, and are spatially associated with large-scale faults which probably occur in a km-spaced network (Thury et al. 1994). As such, the basement can be described as a fractured aquifer.

Schmassmann et al. (1992) established that the basement and Buntsandstein aquifers are hydraulically connected,

constituting a single aquifer system of regional extent. However, the strong heterogeneity of this system needs to be underscored. The basement is dissected by numerous Permo-Carboniferous troughs of local to subregional scale, with the result that the Buntsandstein does not always cap the crystalline basement. Where it overlies the Permo-Carboniferous clastics it represents an independent aquifer (Schmassmann et al. 1992). In such cases the effective aquifer is confined to the Buntsandstein itself. Schmassmann et al. (1992) emphasize that the basement rocks that are unaffected by brittle deformation have low permeability, thus the regional water circulation in the basement is limited to the discrete zones of enhanced conductivity. The circulation system is also strongly influenced by the location of the Permo-Carboniferous troughs, which act as hydrogeologic barriers. Owing to the high heterogeneity of the basement aquifer, its possible contribution to the overlying Bundsandstein has not been included in the map in Fig. 5b.

Where there is no mixing with the basement waters, the Buntsandstein water is expected to be brackish. In the basement at the northern border of the SMB the water salinity is generally low (around 2 g/L) because it derives from groundwater that has infiltrated through the Black Forest massif (e.g. Schmassmann et al. 1992; Michard et al. 1996). South of the line Basel–Tiegen, few analyses are available and the formation water could be much more saline. The salinity of the Basement water also changes near the Permo-Carboniferous troughs, which contain stagnant, highly saline brines (Pearson et al. 1991; Schmassmann et al. 1992).

The Buntsandstein is succeeded by the Wellengebirge Formation, composed of dolomitic or calcareous mudstones including sand lenses. Its thickness reaches 10–40 m, increasing westwards as far as Aarau. Although these lithologies mostly have low permeabilities, it is the overlying Anhydrite Group of the Middle Muschelkalk, composed of anhydrite with intercalations of dolomitic mudstones and minor rock salt, that seals the Buntsandstein. It has very low permeability and a regional lateral extent. In the SW it is fully 150 m thick, but towards the NE it decreases to 40 m, a thickness which is near the lower limit recommended for caprocks (Table 2). The plasticity of rock salt favours self-sealing processes, which ensure very low permeability. However, the high aqueous solubility can lead to severe subsurface erosion if the salt comes into contact with undersaturated formation water. Anhydrite also has very low permeability, but its rheological behaviour is more brittle. Water infiltration (e.g. along faults) would convert anhydrite into gypsum and provoke swelling, which in turn could seal the faults. However, gypsum is also highly soluble and subject to karstification. The intercalated mudstones have low permeability.

Upper Muschelkalk/Gipskeuper (No. 3 in Fig. 3) The Upper Muschelkalk consists of limestones and marls in its lower half (Hauptmuschelkalk) and of dolomite (Trigonodus Dolomit) in its upper half. Only the latter possesses the properties of an aquifer. Despite a high porosity of around 20%, the permeability is usually lower than 60 mD. According to Signorelli and Kohl (2006) and Küpfer et al. (1989) the aquifer properties are not determined principally by the primary porosity but largely by dissolution, (micro-) faulting and karstification features. Depending on the spatial intensity of this secondary porosity, the hydraulic transmissivity changes by several orders of magnitude (10^{-3}–10^{-7} m^2 s^{-1}). According to Biehler et al. (1993), the salinity of the Upper Muschelkalk is highly variable (at least in Northern Switzerland, the studied area). Formation water of low salinity is observed in the Folded and Tabular Jura. Rapid water circulation is expected there, with local infiltration and discharge. At the southern border of the Folded Jura, where the layers dip steeply, waters of different ages and compositions mix, resulting in a relatively higher but still low absolute salinity (Pearson et al. 1991; Biehler et al. 1993). However, in the SMB, borehole data show that the aquifer contains brackish and saline waters of Na–Ca–SO_4-type, which are dominantly due to dissolution of evaporitic gypsum in the Gipskeuper.

Between 800 and 2,500 m depth the Upper Muschelkalk is present as a broad band running along the foot of the Jura between Lake Constance and Yverdon (Fig. 5c). Its thickness is remarkably uniform at about 60 m.

The Upper Triassic is composed of a thin, calcareous claystone sequence (Lettenkeuper) overlain by anhydrite (and massive rock salt in the SW), alternating with clay and marls (Gipskeuper). This unit increases in thickness from 40 m in the NE to about 100 m near Olten and probably to more than 200 m in the SW, due in part to tectonic thickening. It has a very low permeability, providing an extensive seal. The rheologies of the anhydrite, rock salt and claystones are comparable to those of the Anhydrite Group.

Upper Malm/Lower Freshwater Molasse (USM) (No. 6 in Fig. 3) The Malm aquifer consists of karstified limestones of Late Jurassic age (Late Oxfordian to Kimmeridgian). The Late Oxfordian formations are quite variable from reef to argillaceous limestones. During the Kimmeridgian, massive limestones were deposited on the European shelf. In the area of interest they reach a mean thickness of 200 m and consist mainly of micritic limestone. In the far east and towards the Alpine border they become more bituminous.

The matrix porosity and permeability of the Malm are rather low. The unit is nevertheless considered to be an important regional aquifer where the karst conduits preferentially follow bedding and fractures. Eocene marls and

clays (Bohnerz regolith) locally clog these conduits, rendering the aquifer properties highly heterogeneous. Nevertheless, Signorelli and Kohl (2006) estimate a mean hydraulic transmissivity of 10^{-6} m^2 s^{-1} in undisturbed zones and 10^{-5} m^2 s^{-1} in fractured zones in the north and NE of the basin. In the SW, these values are an order of magnitude higher (Beaujard et al. 2006).

Within the 800–2,500 m depth interval the Upper Malm stretches the entire length of the SMB, its thickness varying from about 150–300 m near Lake Constance, thinning to 50 m between Zürich and Olten, then thickening again to around 900 m at Lake Geneva (Fig. 5d).

The overlying Lower Freshwater Molasse (USM) contains local aquifers in a low-permeability matrix. It is dominated by fluvial deposits and therefore has a highly heterogeneous character. From south to north it is characterised by radially prograding gravel fans (conglomerates), braided streams (sandstones) and flood plains (siltstones and mudstones). Its freshwater limestone and coal seams accumulated in extensive lakes and swamps in the distal parts. Aquifers in the USM are limited to sandstone channels and conglomerates in the proximal area, and to freshwater limestones in the distal areas (Keller 1992). The thickness of these water-bearing members varies from a few m to several tens of m, while laterally they typically extend over several hundreds of m (the limestones may extend up to a few km). The argillaceous members, which formed in flood plains, lakes and swamps, constitute hydrological barriers. As a consequence of the deposition pattern, the vertical hydraulic conductivity is significantly lower than the horizontal conductivity. The connectivity between the small aquifers is the critical parameter in defining the sealing capacity of this heterogeneous formation on the regional scale.

Schmassmann (1990) suggests that the whole Cenozoic wedge of the SMB and the underlying Malm aquifer can be described by one hydrogeologic model. Between the current surface and the Malm Formation, three types of water can be distinguished, evolving from fresh water through brackish to saline waters. Their mutual boundaries are gradational and they run discordant to lithologic contacts. These observations show that the hydrologic seal between the Malm and the surface may not be effective at a truly regional scale. This uncertainty must be borne in mind when viewing the extent of the "sealed" aquifer mapped in Fig. 5d.

Assignment of classes to the intrabasinal evaluation criteria

The foregoing has established that the SMB–Jura contains two or three promising aquifer–seal pairs of regional extent and numerous less extensive candidates for CO_2 storage. Attention is now focused on the nine geological attributes that will be used to rank their potential. In the following the states and variations of these attributes throughout the SMB–Jura are described and divided into broad classes (labelled A, B, C, D; Table 3), which allow portrayal on basin-scale maps. The suitability of the classes for CO_2 storage increases from A (unsuitable) to C or D (highly suitable).

Criterion 1a: Depth to sealed aquifer

As stated in "Geological requirements of a storage site", the depth of a sealed aquifer affects its storage capacity and the mobility of CO_2. Depths <800 m are unfavourable because CO_2 will be in a low-density, gas-like state, which strongly reduces storage efficiency. In addition, the associated high buoyancy and low viscosity under these conditions (Fig. 1c–e) shortens the containment period of a CO_2 plume within a stratigraphic trap. On the other hand, injecting deeper than approximately 2,000 m brings only marginal advantages. For geothermal gradients below 35°C km^{-1} the aqueous solubility remains almost constant (Fig. 1e) and the density of CO_2 even decreases slightly (Fig. 1c), thus storage capacity does not improve with depth. The only advantages of greater depth are the smaller differences in viscosity and density between the CO_2 fluid and the coexisting brine (Fig. 1c, d). However, these gains in reduced mobility of the CO_2 plume are likely to be offset by higher drilling costs and higher energy requirements for compression (Bachu 2003).

Accordingly, for the intrabasinal evaluation in which the entire sedimentary filling of the SMG–Jura is treated as one object, two classes are defined for the depth criterion in Table 3: (A) depth $\geq$ 2,500 m and (B) depth 800–2,500 m. These classes correspond to two geographic zones when projected onto the surface of the SMG–Jura (Fig. 6a): The zone in which at least one sealed aquifer lies within the 800–2,500 m depth interval is the most favourable and therefore it is coloured green; the zone in which all the sealed aquifers lie deeper than 2,500 m is less favourable and therefore it is coloured red. The northern boundary of the green zone is set by the 800 m isohypse to the deepest aquifer, the Top Bundsandstein (Fig. 5c). The green/red boundary is defined by the southern edge of the OMM shown in Fig. 5b, combined with the 2,500 m isohypse to the next sealed aquifer moving down the stratigraphic column, namely, the Lower Cretaceous–Upper Malm (Fig. 5e). The remaining portion of the SMB–Jura, in which all the aquifers are shallower than 800 m (Basel–Schaffhausen), is not considered further in the evaluation of storage potential and it is left uncoloured in Fig. 6a.

Criterion 1b: Aquifer thickness

If the porosity and permeability of the rock and the salinity of the formation water are all uniform throughout an

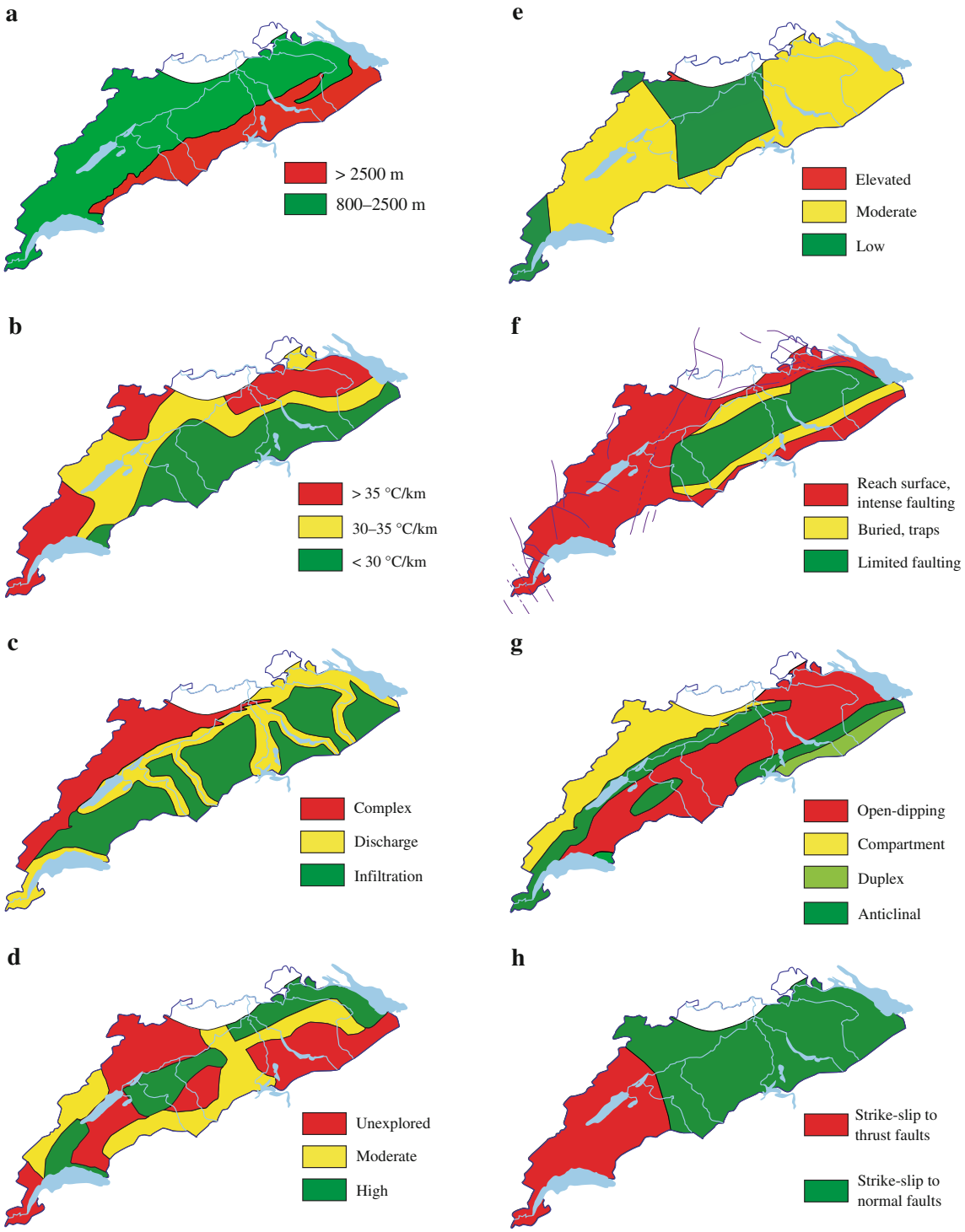

Fig. 6 Maps of the Swiss Molasse Basin and adjacent Jura Domain illustrating spatial variations of selected geological properties relevant to CO_2 storage. Each property is divided into two, three or four classes spanning a range in suitability for CO_2 storage (Table 3): unsuitable (*red*), moderately suitable (*yellow* to *light green*), and highly suitable (*dark green*). Sources of information given in text **a** Depth to sealed aquifer. **b** Geothermal gradient. **c** Hydrogeology. **d** Exploration maturity. **e** Seismicity. **f** Fault systems. **g** Structural traps. **h** Stress regime

aquifer, then its thickness is directly proportional to the amount of CO_2 that it can store. As mentioned in "Methodology for intrabasinal evaluation", the available well data on aquifers in the SMB are too sparse to allow realistic three-dimensional mapping of these parameters. Consequently, for the purposes of this preliminary evaluation we

simply assume that the aquifers possess uniform properties with values above the cautionary limits in Table 2. To provide a rough impression of possible storage capacities in the SMB–Jura, the vertical thicknesses of the main sealed aquifers are shown in Fig. 5, based on the maps in Sommaruga and Eichenberger (2010) and on unpublished borehole and seismic data from the Swiss oil/gas industry. The thinnest portions of the aquifers are coloured red to indicate their lower nominal storage capacities. Thicker portions grade through yellow (intermediate capacity) through to green, which marks the maximum thickness and hence the highest nominal capacity for CO_2.

For the intrabasinal evaluation in which each aquifer is considered alone, it is convenient to distinguish two classes for this criterion in Table 3: (A) sealed aquifers with a thickness less than the 20 m cautionary limit in Table 2; and (B) the maximum thickness of the formation. Areas with thicknesses between the maximum and the 20 m minimum will be assigned different scores for the evaluation ("Assignment of scores").

Criterion 2: Geothermal gradient

As mentioned in "Principles of CO_2 storage in saline aquifers", the in situ temperature of a potential formation is of importance because, along with pressure, it affects the density and viscosity of the injected CO_2 and of the formation brine (Fig. 1). These parameters in turn determine the mobility of the CO_2 plume and the mass of CO_2 that can be stored in the available porosity (Bachu 2003).

According to Rybach et al. (1981) and Rybach (1992) the mean geothermal gradient of the SMB is around 30°C/km, a value which nominally corresponds to the "cold basin" class of (Bachu 2003). However, the gradient varies considerably from place to place, as shown by the three broad subdivisions in Fig. 6b: (A) above 35°C/km, (B) 30–35°C/km and (C) below 30°C/km. The Geneva area has a high gradient close to 40°C/km. In the Folded Jura the gradient is around 35°C/km. Gradients of 25°C/km are common in the southern part of the basin. The Rhine Graben is a well known thermal anomaly (45°C/km) with a clear continuation to the SSW along the prolongation of the rift structure (Rybach 1992). The anomalous zone reaches south to at least the area of Bienne. Two other pronounced "hot spots" (>45°C/km) are located near the confluence of the Aare, Reuss, and Limmat rivers in the south, and near the confluence of the Aare and Rhein in the north. Both anomalies are situated on the flanks of the Konstanz–Frick Permo-Carboniferous trough (also known locally as the Weiach trough; Nagra 2002). The enhanced gradients are therefore attributed to deep formation water ascending along the fault-bounded flanks of the trough (Rybach et al. 1987), driven by large differences in hydraulic potential between the recharge and discharge zones (Thury et al. 1994; Nagra 2002). Similar local thermal anomalies are possible in other parts of the basin close to fault systems (not shown in Fig. 6b). The thermal spa of Yverdon, for example, takes advantage of deep formation water ascending along the Pipechat–Chamblon–Chevressy fault system (Muralt et al. 1997).

Criterion 3: Hydrogeology

Few hydrogeological investigations have been carried out on a regional scale within the SMB except, again, in NE Switzerland where models were developed for the Nagra projects (e.g. Kimmeier et al. 1985). This research has shown that the hydrogeology is complex and that is it difficult to draw a regional picture of groundwater flow directions and residence times. Hydrogeologic complexity and heterogeneity are evident in the descriptions of the various regional aquifers presented above. Nevertheless, it is possible to define some broad hydrogeological domains from the regional model developed by Bouzelboudjen et al. (1997), as shown in Fig. 6c. This model is based on the theoretical studies of Toth (1995), which consider local, intermediate and regional flow systems between conjugate recharge and discharge areas.

The SMB is characterized by important discharge areas that correspond to the major drainage system. These zones drain rocks at considerable depths and so strong upwelling is to be expected. The major discharge zones are the Rhone, the Aare and the Rhine valleys. Other important discharges are the Thur, the Limmat, the Reuss, the Emme and the Seeland (lakes Neuchâtel and Bienne). Discharge zones acting at an intermediate scale include, for instance, the Töss, the Wigger and the Sarine. Infiltration and translation fluxes occur between the discharge zones, and an important divide (Rhone–Rhein) is situated along the line Echallens–Châtel-St-Denis. Large structural disturbances affect and add complexity to this general picture. Examples are the main thrust zone of the eastern Folded Jura, which causes groundwater mixing, and the Konstanz–Frick Permo-Carboniferous trough, which represents a N–S hydrogeologic barrier for the basement (Schmassmann et al. 1992).

In the Folded Jura the complexity of the hydrogeologic systems does not permit a regionally valid simplification as in the case of the SMB. Karst conduits play a key role, in some cases draining entire basins (e.g. the Joux or the Sagne closed valleys). Current knowledge is insufficient to discern the behaviour of potential aquifers confined at greater depths.

In the Tabular Jura, the recharge occurs through outcrops in the elevated zones and discharge occurs in the incised valleys or in the regional discharge zones of the Rhine and the Aare rivers.

Overall, the various hydrogeologic regimes can be grouped into three classes (Fig. 6c): (A) zones with complex hydrogeologic regimes that are difficult to characterize (e.g. Jura), (B) regional discharge zones and (C) the intervening infiltration zones. We neglect the intermediate and local-scale systems, as their water fluxes become insignificant at depths approaching those of interest for CO_2 storage.

Criterion 4: Exploration maturity

Some 35 deep boreholes were drilled and 8,500 km of seismic lines were shot over the course of three decades of oil and gas exploration in Switzerland between 1956 and 1989 (Lahusen 1992). Except for one small gas field in Entlebuch (Vollmayr and Wendt 1987), no commercially exploitable reservoirs were found. This has had two consequences. First, without any return on the investment that was made, further exploration has been considered too risky, leaving the basin at an undeveloped level. Second, the acquired data represent the only asset of the investors, and so access to about 50% of the data is restricted. Assorted information on various aspects of the subsurface has been assembled during other commercial ventures (geothermal energy, salt production, civil engineering, etc.), but even where publicly available, the information is widely dispersed, rendering a detailed compilation a formidable task. Consequently, for our geographical differentiation of the exploration maturity of the basin we rely on the map compiled by Nagra (Annex 2.1-1 in Nagra 2008), which shows the locations of all boreholes deeper than 300 m and of all seismic lines.

Thus, three classes of knowledge of the underground are distinguished (Fig. 6d): (A) the unexplored areas with very little information in the east of the Folded Jura, the west of the Tabular Jura, and the south and SE of the Plateau Molasse; (B) areas with moderate density of well and seismic data, and (C) the best explored areas with comparatively abundant information in the NE of the basin, the central part between Fribourg and Olten, and the Lausanne–Yverdon area.

Criterion 5: Seismicity

In a review of the seismicity of Switzerland, Nagra (2008) concluded that earthquakes are not predicted well if only recent recordings and paleoseismic evidence are used as a basis. These types of information need to be coupled with a probabilistic analysis (e.g. Abrahamson 2000). Abrahamson et al. (2004) and Giardini et al. (2004) developed such a model for Switzerland. Their results allow three zones of activity to be defined in the SMB and adjacent Jura (Fig 6e): (A) elevated seismic activity is concentrated in the Basel area along the Upper Rhine Graben; (B) moderate activity characterizes the eastern and western parts of the SMB (including the central Folded Jura), while (C) minor activity is recorded in the central part of the SMB (including the east of the Folded Jura and the Tabular Jura) and the Geneva area.

Criterion 6: Fault systems

Faults pose a delicate problem for CO_2 storage. They have the contradictory abilities to either create structural traps for fluids or to provide pathways for fluid circulation. Consequently, the simple knowledge of the existence of faults in a given region is an insufficient basis for an evaluation. To distinguish the possible role that they may play in CO_2 storage, knowledge of their activity, extent and structural style is essential. The SMB and adjacent Jura are affected by numerous fault systems, some of which are visible at the surface, whereas others terminate within the Cenozoic or Mesozoic strata. The occurrence of many of the faults, if not all, can be ascribed to reactivation of older Paleozoic lineaments (e.g. Gorin et al. 1993; Müller et al. 2002; Allenbach and Wetzel 2006).

For the purposes of evaluating CO_2 storage potential, the descriptions and interpretations of faults in the literature allow three classes of faulted zones to be distinguished (Fig. 6f): (A) zones with high fault density and/or with faults that dominantly cut through the entire sequence of lithologies, including those that are known to favour leakage (e.g., as evidenced by ascending formation water) or that are potentially active (e.g., as evidenced by recent seismicity or fault movements); (B) zones with faults that generally do not reach the surface and which may be related to favourable structural traps at depth; and (C) zones with only little evidence of faulting. The occurrences of these zones are summarized in the following with reference to the major faults labelled in Fig. 1.

Along the northern boundary of the basin the strata of the Tabular Jura are largely undisturbed. Important exceptions are the dominantly N–S Rhenish lineaments near Basel, and the area near Schaffhausen at the NE limit of the SMB. Here a series of steep normal faults appear, running NW–SE as far south as Lake Constance (nos. 14–16 in Fig. 1a). They evolved between the Pliocene and the Present from purely extensive into dextral transtensive systems (Müller et al. 2002). There is no unique lineament but rather several complex branches, each with its own motion. The faults originate in the basement and show signs of recent seismic activity (Müller et al. 2002). The southern border of the Tabular Jura is marked by the E–W-trending Front Thrust (no. 11 in Fig. 2a), a fault zone that drains deep formation water, as evidenced by the presence of thermal springs (Vuataz 1982; Schmassmann et al. 1984; Bodmer and Rybach 1985).

The Folded Jura is dissected by a set of NNW–SSE wrench faults (nos. 1–9 in Fig. 2a). Most extend into the SMB, as revealed by seismic studies (e.g. Gorin et al. 1993; Signer and Gorin 1995; Sommaruga 1999). In general these faults show sinistral motion and smaller dextral NE–SW systems are sometimes conjugated to them (Mosar 1999; Sommaruga 1999). They affect the whole Mesozoic and Cenozoic stack. While Signer and Gorin (1995) postulate involvement of the basement, Sommaruga (1999) considers the faults to be Paleozoic lineaments that were rejuvenated as tear faults during the Jura folding, without mobilisation of the basement (the faults die out in the Triassic detachment horizon). Recent seismic activity is attributed to some of these systems (e.g. Thouvenot et al. 1998; Gorin et al. 2003). They may also represent zones of enhanced water circulation (e.g. Muralt et al. 1997).

The steep NNE-striking faults along the line Fribourg–Basel (no. 10 in Fig. 2a) are thought to be part of a southward continuation of the Rhenish lineament under the SMB. This interpretation is supported by several points of evidence, including the N–S dissection of the Jura chain, seismic activity in the Fribourg syncline, bending of the anticlinal flexures in this area from NE–SW to N–S, and sedimentological features (Allenbach and Wetzel 2006; Kastrup et al. 2007). Giardini et al. (2004) and Kastrup et al. (2007) postulate that the Fribourg fault has been recently active.

The southern border of the Folded Jura gives way to a structurally distinct strip, about 10 km wide, known as the Sub-Jura Zone. It is characterized by a series of anticlines that are narrower and that have higher amplitudes than those in the remainder of the Plateau Molasse. These structures represent potential traps (see below). The anticlinal geometry affects the entire sedimentary filling of the basin. However, the associated faults seem to affect principally the Mesozoic strata, terminating inside the Cenozoic units. The faults are interpreted to originate either in the basement or in the Triassic detachment horizon, usually involving a passive role of the basement (e.g. Diebold et al. 1991; Gorin et al. 1993; Sommaruga 1999).

The flanks of the Konstanz–Frick trough in northern Switzerland are delimited to the north and the south by near-vertical faults running E–W. The faults were obviously reactivated, since they affect the entire overlying sediment stack. At the surface they are identified as the Baden–Irchel–Herdern lineament to the south and the Rafz-Marthalen flexure to the north (nos. 12 and 13 in Fig. 2a; Müller et al. 2002).

The central part of the Plateau Molasse is sparsely affected by faults. However, seismic evidence indicates the presence of steep subvertical faults with minor displacement in the buried Mesozoic strata. They generally originate in the basement and terminate somewhere in the Cenozoic sediments (e.g. Diebold et al. 1991; Gorin et al. 1993; Pfiffner et al. 1997). A spacing of a few km between large faults is typical in the east and south-west, whereas the spacing increases to 10 km or more in the central area between Bern and Lucerne.

At the transition towards the Subalpine Molasse, folds and thrusts are present in the Cenozoic sediments. In general the thrusts are steep at the surface and flatten out at depth within the Cenozoic wedge or at its base (Micholet 1992; Vollmayr 1992; Pfiffner et al. 1997). A kilometric spacing between the thrusts is typical. In the underlying Mesozoic stack it is expected that normal or reverse faults delimited by strike-slip faults (flower structures) are present, emanating from the basement (Vollmayr 1992; Gorin et al. 1993; Signer and Gorin 1995; Pfiffner et al. 1997). The latter structures provide traps for fluids, as was the case at Entlebuch, the only site of commercial gas production so far within Switzerland (Vollmayr and Wendt 1987).

Criterion 7: Structural traps

Structural traps are not a prerequisite for CO_2 storage, since the immiscible CO_2 plume can be confined for long periods by the caprock of the aquifer. However, effective trap structures have the advantage of constraining the injected CO_2 to a limited area, which reduces the amount of investigation needed to establish confidence for an injection site and which facilitates post-injection monitoring. In Switzerland detailed knowledge of traps is limited because of the general lack of exploration and because of the restricted access to exploration data. Nevertheless, the published data allow recognition of three classes of potential trap features (Schegg et al. 1997) as shown in Fig. 6g: (A) areas without known traps, consisting of open-dipping strata; (B) tilted fault compartments in extensional and compressional settings, mainly at the Paleozoic–Triassic transition below the Folded or Tabular Jura or in the Mesozoic–Lower Tertiary level (areas of Kreuzlingen, Pfaffnau or Essertines–Yverdon); (C) overthrusted duplex structures within and below the Subalpine Molasse (e.g. triangle zone of Eastern Switzerland) or in the lower Mesozoic strata in the external part of the SMB (e.g., north of Lindau or south of Pfaffnau); (D) various anticlinal structures such as the gentle folds in the Tertiary (mainly in an intermediate basin position along the line Fribourg–Bern), and the deep Mesozoic folds beneath the Subalpine Molasse (line St. Gallen–Luzern–Entlebuch) or those related to shallower mega-anticlines (Essertines, Cuarny, Hermrigen, Berlingen–Kreuzlingen).

Criterion 8: Stress regime

According to Bachu (2003), thrust regimes are less favourable for CO_2 storage than extensional regimes,

owing to their generally higher structural complexity and prevalence of non-sealing (leaky) faults. In accord with this view Brink et al. (1992) attribute the paucity of preserved oil and gas accumulations in the SMB largely to its compressional structural style and stress regime. In contrast, the German Molasse Basin is relatively rich in hydrocarbons, and there the tectonic regime is extensional. Despite the overall less favourable setting of the SMB, important regional differences in stress regime can be distinguished within its boundaries, and these can be used as criteria for site selection.

Kastrup et al. (2004) assessed the present-day stress regime in the Northern Alpine Foreland from the inversion of fault-plane solutions. The compression axis lies perpendicular to the Alpine Front. Hence it undergoes a 45°–50° rotation as the Front bends from SW–NE in the west to W–E in the east of the SMB. The areas currently with different stress regimes are shown in Fig. 6h: (A) in the Geneva area the dominant stress state corresponds to a less favourable strike-slip to thrust faulting regime; (B) east of Solothurn and further to the NE, more favourable strike-slip to normal faulting (extension) dominates. The area between Lausanne and Bienne shows similar results to the Geneva area, but no inversion could be performed there (Kastrup et al. 2004).

Parameterization of the geological evaluation criteria

In this section the nine criteria valid at the intrabasinal scale are parameterized to enable numerical evaluation. Following Bachu (2003), the classes within each criterion are assigned scores between 1 (unsuitable for CO_2 storage) and 15 (maximum suitability). The progression of scores between classes is determined by specified mathematical functions, as described below. Finally, each criterion is assigned a weighting factor based largely on subjective arguments.

Assignment of scores

Table 3 lists in square brackets the scores assigned to the classes within each geological criterion. These scores are based on the following reasoning.

The simplest function that could be used to assign scores is linear, because it represents a steady increase in suitability of each successive class. This is appropriate for the variation in thickness of an individual aquifer, assuming, as done here, that its storage properties are uniform. A linear progression is also suitable for the geothermal gradient, because below about 1000 m the CO_2 density, viscosity and aqueous solubility all decrease roughly linearly with increasing gradient (Bachu 2003; Fig. 1c–e). Owing to the ambiguous role of buried faults, which may enhance leakage or trapping of CO_2, a linear function for the fault-systems criterion also seems reasonable.

Assigning an exponential function causes the score to increase moderately between classes A and B, and then increase by a large amount between B and C. This corresponds well to the criteria of hydrogeology and seismicity, where the best class favours CO_2 storage far more than the others.

A logarithmic dependency, in contrast to the exponential function, shows a strong increase between classes A and B, while the rate of increase flattens out towards higher classes. This is appropriate for the criterion of exploration maturity, where moderate knowledge of the subsurface is a vastly better basis for assessment than almost no knowledge. The classes for structural traps are also related in a similar way, there being a great difference between no trap at all (open-dipping structures) and any kind of trap, but no large difference between one kind of trap and another. A logarithmic function would also be appropriate for the stress regime, in principle. However, as only two classes could be differentiated, the type of function chosen is irrelevant.

The depth-to-sealed-aquifer criterion is represented by a parabolic function, as the optimum depth range for CO_2 storage corresponds to a mathematical maximum. All other factors being equal, drilling deeper will not bring substantial advantages but it will increase costs.

Assignment of weighting factors

The purpose of weighting the various criteria is to take account of their relative importance and of the reliability of the information on which they are based. The criteria are ranked in Table 3 according to the weights resulting from the following considerations.

The two most important criteria are the presence of a sealed aquifer within the optimal range of injection depths and the thickness of the aquifer. Hence both are assigned weights of 0.2. The regional hydrogeological regime is equally important, but in the SMB and Jura it is only poorly defined and so it is weighted 0.15. The geothermal gradient is significant owing to its control on injection depth and storage capacity, and the database is relatively well founded, hence it is also assigned a weight of 0.15. The exploration maturity has a similar impact, because it determines confidence in the final assessment of storage potential. Thus, it too is weighted 0.15. Seismicity, fault systems and the presence and nature of structural traps are all assigned the same weight, as they are phenomenologically related to each other. However, because detailed information on these three criteria is lacking in the SMB and Jura, they are each weighted 0.10. The stress state receives the lowest weight, 0.05, because it is poorly constrained.

It can be seen in Table 3 that the weights of the nine criteria sum to 1.2, rather than 1.0 (cf. Table 1). This sum has been chosen purposefully to facilitate the two different kinds of intrabasinal evolutions: one that excludes criterion 1b and one that excludes 1a. Thus, in each case the weights sum to 1.0.

Calculation of normalized potentials

In order to calculate the total storage potential for a given case, the scores are first normalized by the factor

$$\frac{(\text{score} - 1)}{(\text{maximum score} - 1)},$$

where the maximum score is 15 and where 1 is subtracted from both numerator and denominator to render the scores for the "unsuitable" class A equal to 0. The normalized scores for each criterion are then multiplied by their respective weights and summed to yield a potential between 0 (negligible potential) and 1 (excellent potential). This numerical scale is readily transformed into a colour scale for display on maps.

Results: potential of the SMB–Jura for CO_2 storage

Basin-wide potential

In this first evaluation the scheme of Bachu (2003) is applied to the SMB–Jura without modification (Table 1). The classes that in our assessment best fit the Swiss case are italicized in Table 1, resulting in a score of 0.6. Thus, the SMB–Jura falls between the scores for the Alberta Basin (0.96) and the St. Lawrence Basin (0.31), which are given as examples in "Methodology for basin-wide evaluation" above. As the maximum score in this scheme is 1.0, the CO_2 storage potential of the SMB, when viewed as a whole, can be described as moderate.

Intrabasinal potential of the entire sedimentary stack

In this second evaluation, all the maps shown in Fig. 6 are combined using the scores and weights given for the corresponding criteria 1a and 2–8 in Table 3 (criterion 1b in Table 3 is ignored). Thus, the CO_2 storage potential of the entire sedimentary filling of the SMB–Jura is projected onto a map surface in Fig. 7 to provide geographic differentiation at the scale of a few km^2. The weighted merger of the maps in Fig. 6 and the subsequent contouring was performed with a standard digital mapping procedure.

The calculated scores vary between 0.26 and 0.96, with a mean of 0.53, and their map distribution reveals clear patterns (Fig. 7). Considering all the sealed aquifers simultaneously, the best potential for CO_2 storage lies in the green belt Fribourg–Bienne–Baden–St. Gallen. While antiformal traps are thought to be present along its northern rim and in the Fribourg–Bern area, the rest of the belt is characterized by open-dipping structures (Fig. 6g). This suggests that stratigraphic trapping may be the best option for CO_2 containment in this area, although not all sectors have been well explored yet (Fig. 6d). South of the green belt the storage potential is disfavoured by the great depth of the aquifers, by the low exploration maturity, and by the intensity of faulting near the Alpine Front (Fig. 6a, d, f). The entire Jura seems to have only weak potential, despite the presence of some aquifers. The zone is disqualified by the combination of unsuitable geothermal gradients, hydrogeology, exploration maturity, fault systems and stress regime (cf. Fig. 6). Similarly, the region between Lausanne and Lake Neuchâtel is penalized by poor scores for exploration maturity, fault systems, structural traps and stress regime, with only the favourable depth to aquifers as partial compensation (Fig. 6a, d, f–h). In the SW of the basin, the regions immediately NW and E of Lausanne have good potential, whereas near to and north of Geneva the potential is too low to be of interest.

Overall, the storage potential displayed in Fig. 7 is remarkably favourable. Some 32% of the evaluated area has a score above 0.6. This corresponds to almost exactly 5,000 km^2 of terrain which could be explored in more detail. Only 6% of the SMB–Jura scores above 0.8, presenting a rather small exploration target of around 1,000 km^2.

Intrabasinal potential of individual aquifers

In this third evaluation the maps in Fig. 5 of individual sealed aquifers within the 800–2,500 m depth range are each combined with the maps in Fig. 6b–h. Again, a digital mapping procedure was used to perform the merger and contouring, using the scores and weights given for the corresponding criteria 1b and 2–8 in Table 3 (criterion 1a in Table 3 was ignored). The resulting maps are shown in Fig. 8. Each displays potentials that are relative to the maximum thickness (weight 0.2) of the specific aquifer. Because of this dependency the scores depicted in one map cannot be compared to those in another.

Figure 8a shows that the eastern half of the Hauptrogenstein has much higher potential than its western half. Although the aquifer has comparable thickness in the west, the unfavourable structural attributes (criteria of fault systems, structural traps and stress state) and low exploration maturity render its potential there essentially negligible. The small OMM aquifer shows a strong local variation in potential, its best portion lying very near to the city of St. Gallen.

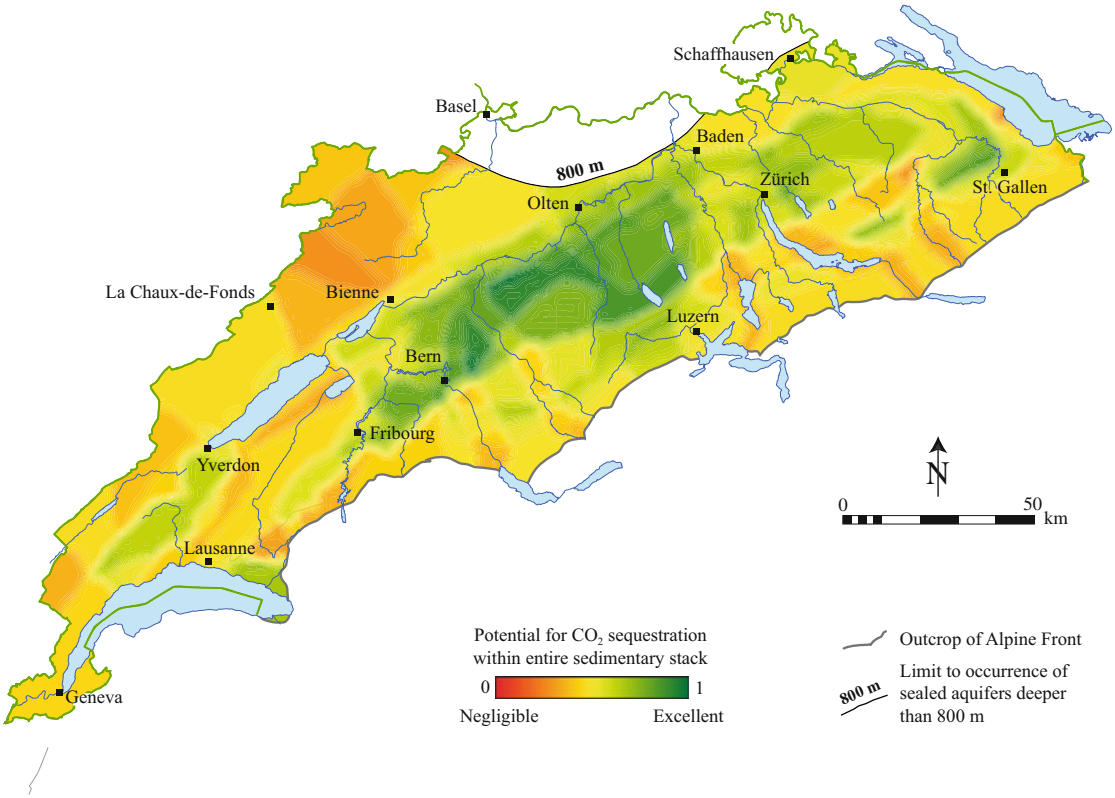

Fig. 7 Intrabasinal evaluation of the potential of the Swiss Molasse Basin and adjacent Jura for geological storage of CO_2. *Colours* show the potential of the entire sedimentary stack below each point in the map. Approximately 5,000 km^2 of the mapped area exhibits storage potentials above 0.6

The Buntsandstein (Fig. 8b) has only moderate potential at best. Throughout virtually the entire area in which the aquifer is more than 20 m thick (cf. Fig. 5b), criteria 2–8 unite to produce weak potential.

Although the thickness of the Upper Muschelkalk aquifer is constant at 65 m, whereas the thickness of the Malm–Lower Cretaceous varies enormously between 50 and 1,200 m, the potential maps of these two aquifers are rather similar (Fig. 8c, d), being largely determined by criteria 2–8 in Table 3. Thus, both aquifers display good to excellent potential in their central regions. Here geothermal gradients, hydrogeology, seismicity, fault systems and stress regime all combine favourably. In contrast, the high geothermal gradient and intense faulting penalize the aquifers in the NE, and their unfavourable structural attributes lower their scores again between Fribourg and Lake Neuchâtel. Small areas with more promising scores up to 0.6 are located in the Muschelkalk south of Yverdon and in the Malm–Lower Cretaceous east and west of Lausanne.

Estimation of CO_2 storage capacity

Theoretical storage capacities for CO_2 can be calculated from the product of the volume of the saline aquifer, the interconnected porosity of the aquifer, and the density of the CO_2 in equilibrium with the ambient temperature and fluid pressure. This theoretical capacity can never be achieved in practice, for two main reasons. First, owing to the physical phenomenon of capillarity, not all the formation water can be expelled from the rock pores when free CO_2 is forced through the formation (the residuum is referred to as the irreducible water saturation). Consequently, the space available for CO_2 is reduced. Second, owing to technical limitations, not all the connected porosity in an aquifer can be infiltrated by CO_2 injected from a borehole. To account for these and other effects, the theoretical capacity can be multiplied by a dimensionless factor (storage coefficient) to obtain the effective storage capacity, as follows:

$$M_{CO_2,\mathrm{eff}} = \int_{800\mathrm{m}}^{2{,}500\mathrm{m}} \left(V_{\mathrm{aquifer}} \cdot \phi_{\mathrm{aquifer}} \cdot \left(\rho_{CO_2}\right)_T \cdot E\right) dz \qquad (1)$$

where $M_{CO_2,\mathrm{eff}}$ is the effective storage capacity for CO_2 (kg); V_{aquifer} is the volume of the aquifer within the depth interval dz (m^3); ϕ_{aquifer} is the interconnected porosity of the aquifer within the depth interval dz (m^3); $\left(\rho_{CO_2}\right)_T$ is the mass-density of CO_2 at the aquifer temperature T within the depth interval dz (kg/m^3); E is the site-scale, effective storage coefficient at aquifer temperature T, within the depth interval dz.

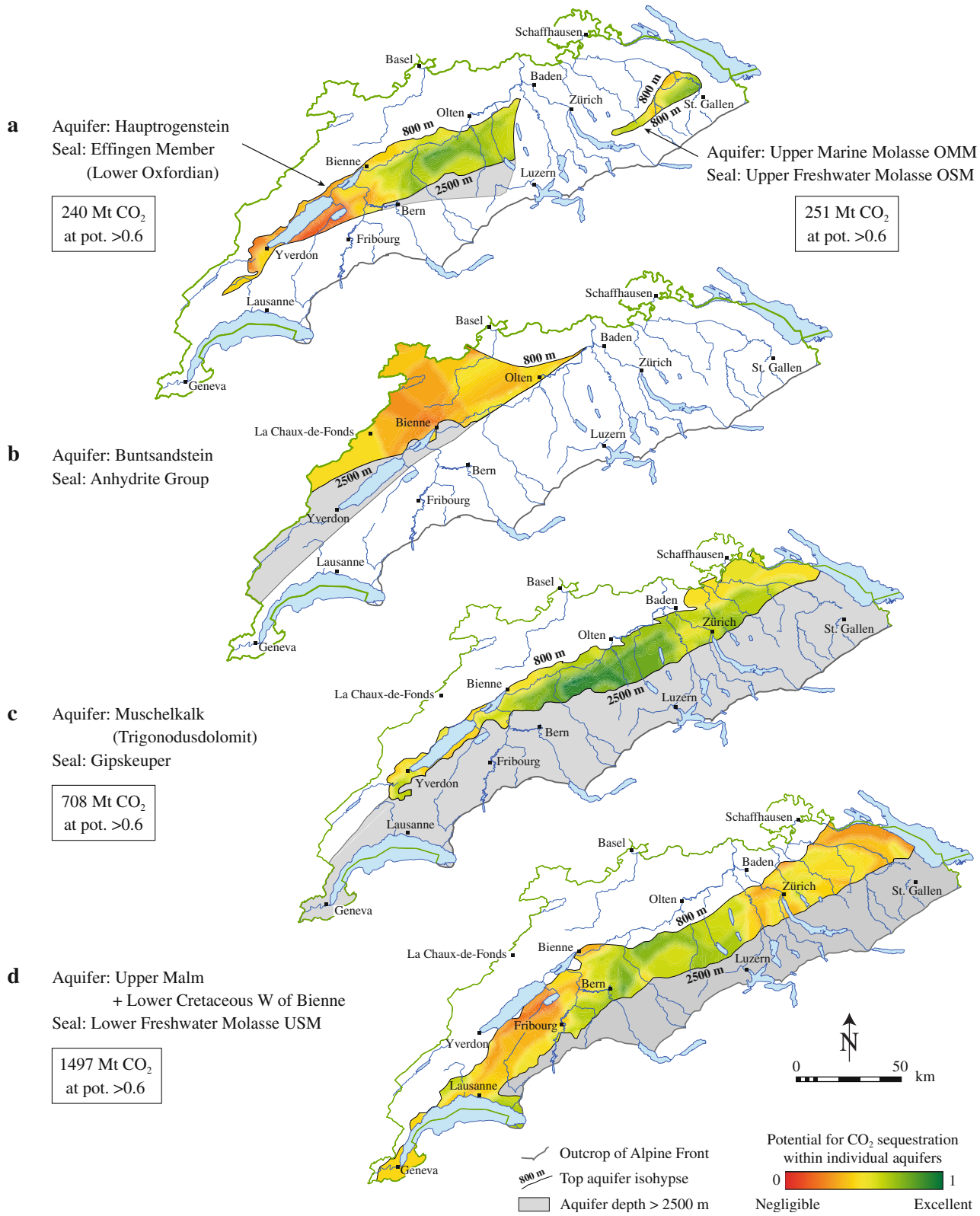

Fig. 8 Intrabasinal evaluation of the CO_2-storage potential of individual sealed aquifers in the Swiss Molasse Basin and adjacent Jura. *Inset boxes* show the theoretical, effective storage capacity of the portions of each aquifer with potential >0.6

Table 4 Input parameters and calculated effective storage capacities of aquifers for CO_2

Aquifers[a]	Upper Marine Molasse	Haupt–rogenstein	Upper Muschelkalk	Malm–Lower Cretaceous
Area with storage potential >0.6 (km^2)	172	1,095	2,088	1,554
Volume of aquifer ($V_{aquifer}$) with storage potential >0.6 in depth interval 800–2,500 m[b]				
<30°C/km (m^3)	1.33×10^{10}	6.35×10^{10}	3.80×10^{10}	5.53×10^{11}
30–35°C/km (m^3)	4.81×10^{10}	3.11×10^{10}	5.30×10^{10}	5.50×10^{10}
>35°C/km (m^3)	1.28×10^{10}	3.74×10^{9}	4.47×10^{10}	3.99×10^{10}
Total (m^3)	7.43×10^{10}	9.83×10^{10}	1.36×10^{11}	6.48×10^{11}
Total (km^3)	74.3	98.3	136	648
Mean interconnected porosity of aquifer $(\bar{\phi})$ (%)[c]	12.5	8.5	8.7	5
Mean CO_2 density $(\bar{\rho})$ in depth interval 800–2,500 m[d]				
<30°C/km (kg/m^3)	740	740	740	740
30–35°C/km (kg/m^3)	675	675	675	675
>35°C/km (kg/m^3)	575	575	575	575
Lithology of aquifer (using available IEA-GHG typology)[e]	Alluvial fan sandstone	Peritidal limestone	Shallow shelf dolomite	Shallow shelf limestone
Structure (attitude of bedding)[e]	5° incline	5° incline	5° incline	5° incline
CO_2 storage coefficient P10 (%)[e]	4.60	4.99	4.99	5.52
[5] CO_2 storage coefficient P50 (%)[e]	4.85	4.97	4.97	7.10
Mean of P10 and P50 coeffs. $(\bar{E})$ (%)	4.7	5	5	6.3
Effective CO_2 storage capacity				
$M_{CO_2,eff}$ calc. from Eq. 2 (Mt)	251	240	708	1,479
Mean $M_{CO_2,eff}$/square km (Mt/km^2)	1.45	0.22	0.34	0.95

Mt millions of tonnes

[a] Excluding Buntsandstein, which has no areas with storage potential >0.6

[b] Calculated from the *vertical thicknesses* and *isohypses* in Fig. 5, and from storage potentials in Fig. 8

[c] Calculated from ranges in Fig. 3, derived from logs of the *deep boreholes* marked in Fig. 5

[d] Depth integration of values plotted in Fig. 1c, based on equation of state of Span and Wagner (1996)

[e] From Appendix E in IEA-GHG (2009)

In the present case, it is meaningful to calculate CO_2 storage capacities only for the portions of the aquifers that show good potentials. Thus, in view of the uncertainties in our method, we have arbitrarily chosen to consider only potentials >0.6. In addition, the rather coarse database available for the aquifers in the SMB–Jura does not justify integrating Eq. 1 with small depth increments (dz). Therefore, the following approximations have been made to estimate mean values of the parameters (Table 4), which permit the storage capacity to be calculated as a simple product. The volumes of the aquifers with potentials >0.6 have been calculated from the vertical thicknesses and isohypses in Fig. 5 for the depth interval 800–2,500 m. For each formation, we have used mean values of the interconnected porosity measured by standard mercury injection and other methods, collated from a variety of published and unpublished logs of the deep boreholes marked in Fig. 5. The ranges of these values are given in Fig. 3. The density of CO_2 depends on the geothermal gradient as well as on the depth, via the hydrostatic pressure (Fig. 1c). As three classes of geothermal gradients have been used to calculate the storage potentials (Fig. 6b; Table 3), each of these classes has been assigned a depth-integrated mean CO_2 density based on the data plotted in Fig. 1c. Generic values of storage coefficients are given by IEA-GHG (2009), based on estimations using a variety of empirical observations and computer simulations. These values can be used for predictive calculations in lieu of field tests at a specific site. Here we have used site-scale values from Appendix E (P10 and P50 estimates) in IEA-GHG (2009), which differentiate lithology, depositional environment, the inclination of the strata, depth, temperature, salinity and other parameters.

All these approximations allow Eq. 1 to be simplified to:

$$M_{CO_2,eff} \approx V_{aquifer,800-2,500m} \cdot \bar{\phi}_{aquifer} \cdot \bar{\rho}_{CO_2} \cdot \bar{E} \qquad (2)$$

where the overbars denote the mean values as explained above. The results are shown in the bottom rows of Table 4 and in Fig. 8 for each of the main aquifers (except for the Buntsandstein, which has no storage potential >0.6). The Malm–Lower Cretaceous aquifer offers the greatest storage

capacity (1,479 million tonnes), owing to its large extent and considerable thickness, whereas the OMM offers the greatest mean capacity per km^2 (1.45 million tonnes), owing to its great thickness and high porosity. The combined effective storage capacity in all four aquifers is 2,680 million tonnes of CO_2.

Discussion

Although the results of this study are encouraging, it should be borne in mind that, for want of published data, our evaluation has not taken explicit account of the critical factors of porosity, permeability, capillary entry pressure of the caprocks and salinity of the formation water (cf. Table 2). Consequently, we rely mainly on the well known, qualitative hydraulic properties of the various formations, and we assume these to be uniform. Judging from the ranges of porosity and permeability in Fig. 3, this seems reasonable for the Hauptrogenstein, Upper Marine Molasse, Buntsandstein and the Upper Muschelkalk. It is less certain for the Malm–Lower Cretaceous, in which matrix porosities and permeabilities are low and in which the spatial extent of karst and fracture porosity is currently unpredictable. This situation reflects the scarcity of data from in situ hydraulic testing within boreholes in the SMB. Many of the aquifers are dissected by systems of joints that strongly influence permeability. However, this influence cannot be assessed by standard measurements of porosity and permeability on drillcore samples.

The above uncertainties make it difficult to compare the potential of the different aquifers. For example, it is conceivable that a 30 m thickness of highly porous Hauptrogenstein could store more CO_2 than a 300 m thickness of poorly fractured Malm. Once more information on the spatial variability of these factors becomes available, the maps of storage potential could change. Similarly, any new deep drillholes or seismic studies in areas with hitherto sparse subsurface information may reveal geological features that require Fig. 7 to be modified, including new local aquifer/seal pairs and perhaps more information on the yet unknown potential of the Permo-Carboniferous troughs.

Another crucial feature of the present study is that the assignment of scores and weights for the various classes of criteria, as explained in "Parameterization of the geological evaluation criteria", is in part subjective. The numerical values are based on our assessment of the available geological data, on the experience of authors in the literature, and on our own experience. Other workers may derive slightly different values from the same information base. However, by having broken down the numerous variables into scored classes with individual weights, slight differences of opinion will not change the overall picture of region potentials.

Conclusions

Switzerland's modest results from hydrocarbon exploration augur poorly for CO_2 storage in natural gas reservoirs, though future exploration may change this situation. Similarly, while coal seams may in principle be used to trap CO_2, the potential for this option in Switzerland cannot be meaningfully assessed at present. The one known borehole intersection with deep, unmineable coal (at Weiach in the Konstanz–Frick trough) is an insufficient basis to predict the size and properties of a potential storage formation. Again, further deep drilling may provide the necessary information to conduct an assessment in the future. In contrast, deep saline aquifers in the sedimentary sequence of the Swiss Molasse Basin and adjacent Jura are a promising target for CO_2 sequestration within Switzerland.

Our broad, qualitative appraisal of the aquifers has addressed three aspects of their storage potential. First, the application of an evaluation scheme that is valid for the entire sedimentary stack ranks the potential of the combined SMB–Jura within the mid-range of basins independently evaluated in an important comparative study in Canada. This demonstrates that the basin-scale attributes of the SMB–Jura are favourable enough for CO_2 sequestration to warrant closer attention.

Second, our evaluation of the sedimentary stack at the intrabasinal scale reveals various geographic regions with poor through to excellent potential (Fig. 7). The central region of the SMB-Jura within the sector Bern–Olten–Luzern has the highest potential.

Third, our evaluation of individual, regional- to subregional aquifers within the technically favoured 800–2,500 m depth interval (Fig. 8) reveals promising potential in certain areas: the Hauptrogenstein aquifer east of the line Bern–Bienne; the Upper Marine Molasse (OMM) near St. Gallen; the Muschelkalk in the area Bern–Bienne–Baden–Zürich; and the Malm from the northeast of Fribourg through to the hinterland of Luzern (Hallwilersee). The Buntsandstein offers only moderate potential at best, and it is therefore the least interesting target for exploration.

The maps of storage potential shown in Figs. 7 and 8 must be applied with care. Their smooth contours convey the impression that they depict quantitative results. However, the assignment of numerical values to the potentials has been used in this study simply as an aid to rank different geographical regions and aquifers; the potentials carry an essentially qualitative meaning nonetheless. A

high score in our maps does not guarantee that CO_2 can be sequestered at that point. Rather, the potential maps show which areas are the most prospective for future detailed investigations. If we view aquifer porosity as a valuable resource, then in mineral-deposit terminology our potentials provide a ranking of "probable reserves".

The combined volumes of the four main candidate aquifers with potentials above 0.6 (Fig. 8) offer a theoretical, effective storage capacity for 2,680 Mt (millions of tonnes) of CO_2. The volumes project onto 5,000 km^2 of the surface of the SMB. Thus, the mean CO_2 storage capacity of the green belt in Fig. 7 is approximately 0.53 Mt/km^2. These storage capacities can be put into the local context by considering that the current annual emission of CO_2 from industrial sources in Switzerland is approximately 11.3 Mt (Table 6 in BAFU 2010). A 400 MWel combined-cycle gas power station would produce approximately 0.7 Mt CO_2/year (assuming 360 kg/MWh and 5,000 h/year operation). Clearly, the expected storage capacity of saline aquifers in the SMB is sufficient to cope with industrial emissions far into the future (e.g. for nominally more than 200 years using the cited emission rates).

We emphasize that only geological criteria have been used in this evaluation. Non-geological factors, such proximity to industrial CO_2 sources, transportation issues, conflicts of use of the subsurface, etc., would need to be included in any site-selection project. Inclusion of these criteria via a numerical scoring scheme is likely to shrink the 5,000 km^2 of terrain which now scores >0.6 in our scale of potentials between 0 (negligible) and 1 (excellent).

From a geological perspective, further efforts to quantify the storage potential in the SMB–Jura should include more detailed evaluation of existing seismic and drillhole data in regions of high potential. Once smaller target areas are identified, new seismic surveys and drillholes may be necessary to delineate traps and potentially leaky fault systems, and to allow hydraulic testing and sampling of the aquifer rocks and their formation waters. These data would then need to be integrated by means of predictive numerical simulations of the physical and chemical consequences of CO_2 injection over various time scales, including dissolution within the carbonate aquifers and the hazard of induced seismicity. The resulting estimates of effective storage capacity would need to be verified in a pilot injection project.

Acknowledgments We are grateful for the support of the Schweizerische Studiengesellschaft für Mineralische Rohstoffe and of the Swiss Federal Office of Energy. Critical comments by Andreas Gautschi, Irina Gaus, Martin Mazurek, Niklaus Waber and an anonymous journal reviewer greatly helped to improve the manuscript. We further acknowledge the access to proprietary well data of the Swiss petroleum industry (SEAG and Swissgas).

References

Abrahamson, N. (2000). State of the practice of seismic hazard evaluation. In: *Proceedings of GeoENG*, pp. 19–24.

Abrahamson, N., Coppersmith, K.J., Koller, M., Roth, P., Sprecher, C., Toro, G.R., Youngs, R. (2004). *Probabilistic seismic hazard analysis for swiss nuclear power plant sites (PEGASOS Project)* (358 pp.). Final Rep. Swissnuclear (Swisselectric), Bern.

Akinfiev, N. N., & Diamond, L. W. (2010). Thermodynamic model of aqueous CO_2–H_2O–NaCl solutions from −22 to 100°C and from 0.1 to 100 MPa. *Fluid Phase Equilibria, 295*, 104–124.

Allenbach, R. P., & Wetzel, A. (2006). Spatial patterns of Mesozoic facies relationships and the age of the Rhenish Lineament: A compilation. *International Journal of Earth Sciences, 95*, 803–813.

Bachu, S. (2003). Screening and ranking of sedimentary basins for sequestration of CO_2 in geological media in response to climate change. *Environmental Geology, 44*, 277–289.

Bachu, S., & Adams, J. J. (2003). Sequestration of CO_2 in geological media in response to climate change: Capacity of deep saline aquifers to sequester CO_2 in solution. *Energy Conversion and Management, 44*, 3151–3175.

BAFU. (2010). *Emissionen nach CO_2-Gesetz und Kyoto-Protokoll (Version 15.04.2010)* (p. 11). Bern: Bundesamt für Umwelt BAFU.

Beaujard, C., Signorelli, S., Kohl, T. (2006). Evaluation du potentiel géothermique suisse, rapport annuel 2006. Swiss Geophysical Commission, 18 pp.

Beaujard, C., Signorelli, S., Kohl, T. (2007). Evaluation du potentiel géothermique suisse, rapport 2007. Swiss Geophysical Commission, 5 pp.

Benson, S. M., & Cole, D. R. (2008). CO_2 sequestration in deep sedimentary formations. *Elements, 4*, 325–331.

Benson, S. M., & Surles, T. (2006). Carbon dioxide capture and storage: An overview with emphasis on capture and storage in deep geological formations. *Proceedings IEEE, 94*, 1795–1805.

Biehler, D., Schmassmann, H., Schneemann, K., Sillanpää, J. (1993). *Hydrochemische Synthese Nordschweiz: Dogger-, Lias-, Keuper- und Muschelkalk-Aquifere. Nagra Technischer Bericht NTB 92-08* (410 pp). Wettingen: Nagra.

Bodmer, P., & Rybach, L. (1985). Heat flow maps and deep ground water circulation: Examples from Switzerland. *Journal of Geodynamics, 4*, 233–245.

Bouzelboudjen, M., Kiraly, L., Kimmeier, F., Zwahlen, F. (1997). Geological and hydrogeological profiles. Part 2. Hydrogeology (3 pp.). Bern: Landeshydrologie und -geologie, BAFU, Plate 8.

Brink, H. J., Burri, P., Lunde, A., & Winhard, H. (1992). Hydrocarbon habitat and potential of Swiss and German Molasse Basin—A comparison. *Eclogae Geologicae Helvetiae, 85*, 715–732.

Büchi, U. P., Lemcke, K., Wiener, G., & Zimdars, J. (1965). Geologische Ergebnisse der Erdölexploration auf das Mesozoikum im Untergrund des schweizerischen Molassebeckens. *Bulletin der Vereinigung schweizerischer Petroleum-Geologen und -Ingenieure, 32*, 7–38.

Chadwick, A., Arts, R., Bernstone, C., May, F., Thibeau, S., & Zweigel, P. (Eds.). (2008). *Book Best practice for the storage of CO_2 in saline aquifers: Observations and guidelines from the SACS and CO_2STORE projects* (p. 267). Nottingham: British Geological Survey.

COM. (2008). *Proposal for a directive of the European parliament and of the council on the geological storage of carbon dioxide and amending Council Directives* (p. 48). Brussels: Commission of the European Communities.

Diebold, P., Naef, H., Ammann, M. (1991). *Zur Tektonik der zentralen Nordschweiz. Interpretation aufgrund regionaler*

Seismik, Oberflächengeologie und Tiefbohrungen Technischer Bericht 90-04 (277 pp). Wettingen: Nagra.

Giardini, D., Wiemer, S., Fäh, D., Deichmann, N., Sellami, S., & Jenni, S. (2004). *Seismic Hazard Assessment 2004* (p. 81). Zurich: Swiss Seismological Service.

Gorin, G. E., Morend, D., & Pugin, A. (2003). Bedrock, quaternary sediments and recent fault activity in central Lake Neuchâtel, as derived from high-resolution reflection seismics. *Eclogae Geologicae Helvetiae, 96*, 3–10.

Gorin, G. E., Signer, C., & Amberger, G. (1993). Structural configuration of the western Swiss Molasse Basin as defined by reflection seismic data. *Eclogae Geologicae Helvetiae, 86*, 693–716.

Gunter, W. D., & Perkins, E. H. (1993). Aquifer disposal of CO_2-rich gases—reaction design for added capacity. *Energy Conversion and Management, 34*, 941–948.

Gwinner, M. (1971). Geologie der Alpen. Stratigraphie, Paläogeographie, Tektonik (477 pp.) E. Schweizerbart'sche Verlagsbuchhandlung.

Harrison, W. J., Wendlandt, R. F., & Sloan, E. D. (1995). Geochemical interactions resulting from carbon dioxide disposal on the seafloor. *Applied Geochemisty, 10*, 461–475.

Hepple, R. P., & Benson, S. M. (2005). Geologic storage of carbon dioxide as a climate change mitigation strategy: Performance requirements and the implications of surface seepage. *Environmental Geology, 47*, 576–585.

Holloway, S. (1997). An overview of the underground disposal of carbon dioxide. *Energy Conversion and Management, 38*, S193–S198.

IEA-GHG. (2009). *Development of storage coefficients for CO_2 storage in deep saline formations (118 pp)*. Technical study report 2009/13. Stoke Orchard (UK): IEA Greenhouse Gas R&D Programme.

IPCC. (2005). IPCC special report on carbon dioxide capture and storage. In: Prepared by working group III of the intergovernmental panel on climate change (442 pp). Cambridge, United Kingdom and NewYork, NY, USA: Cambridge University Press.

Jenny, J., Burri, J.-P., Muralt, R., Pugin, A., Schegg, R., Ungemach, P., et al. (1995). Le forage géothermique de Thônex (Canton de Genève): Aspects stratigraphiques, tectoniques, diagénétiques, géophysiques et hydrogéologiques. *Eclogae Geologicae Helvetiae, 88*, 365–396.

Jordan, P. (2007). *Sammelprofile der Sedimentgesteine der verschiedenen geologisch-tektonischen Einheiten der Schweiz. Arbeitsbericht NAB 07-35* (103 pp). Wettingen: Nagra.

Kastrup, U., Deichmann, N., Frohlich, A., & Giardini, D. (2007). Evidence for an active fault below the northwestern Alpine foreland of Switzerland. *Geophysical Journal International, 169*, 1273–1288.

Kastrup, U., Zoback, M.L., Deichmann, N., Evans, K.F., Giardini, D., Michael, A.J. (2004). Stress field variations in the Swiss Alps and the northern Alpine foreland derived from inversion of fault plane solutions. Journal of Geophysical Research *109*(B1). doi: 10.1029/2003JB002550B01402.

Keller, B. (1992). Hydrogeologie des schweizerischen Molasse-Beckens: Aktueller Wissensstand und weiterführende Betrachtungen. *Eclogae Geologicae Helvetiae, 85*, 611–651.

Kharaka, Y. K., Cole, D. R., Hovorka, S. D., Gunter, W. D., Knauss, K. G., & Freifeld, B. M. (2006). Gas-water-rock interactions in Frio Formation following CO_2 injection: Implications for the storage of greenhouse gases in sedimentary basins. *Geology, 34*, 577–580.

Kimmeier, F., Perrochet, P., Andrews, R., Kiraly, L. (1985). *Simulation par Modèle Mathématique des Ecoulements Souterrains entre les Alpes et la Forêt Noire – Partie A: Modèle Régional – Partie B: Modèle Local (Nord de la Suisse). Nagra Technischer Bericht NTB 84-50* (190 pp). Wettingen: Nagra.

Küpfer, T., Hufschmied, P., & Pasquier, F. (1989). Hydraulische Tests in Tiefbohrungen der Nagra. *Nagra informiert, 11*, 3–4.

Lahusen, P. H. (1992). Hydrocarbon exploration in the Swiss Molasse Basin. *Eclogae Geologicae Helvetiae, 85*, 707–714.

Laubscher, H. (1961). Die Fernschubhypothese der Jurafaltung. *Eclogae Geologicae Helvetiae, 54*, 221–281.

Lindeberg, E. & Bergmo, P. (2002). The long-term fate of CO_2 injected into an aquifer. In: Proceedings of 6th international conference on greenhouse gas technologies, pp. 6, Kyoto.

Lohr, J. (1967). Die seismischen Geschwindigkeiten in der Ostschweiz. *Bulletin der Vereinigung schweizerischer Petroleum-Geologen und -Ingenieure, 34*, 29–38.

Mao, S. D., & Duan, Z. H. (2009). The viscosity of aqueous alkali-chloride solutions up to 623 K, 1000 bar, and high ionic strength. *International Journal of Thermophysics, 30*, 1510–1523.

Matter, A., Peters, T., Bläsi, H.-R., Schenker, F., Weiss, H. P. (1988). *Sondierbohrung Schafisheim. Geologie, Textband. Nagra Technischer Bericht NTB 86-03*(321 pp). Wettingen: Nagra.

Mazurek, M., Hurford, A. J., & Leu, W. (2006). Unravelling the multi-stage burial history of the Swiss Molasse Basin: Integration of apatite fission track, vitrinite reflectance and biomarker isomerisation analysis. *Basin Research, 18*, 27–50.

Mazurek, M. & Peters, T. (1992). Petrographie des kristallinen Grundgebirges der Nordschweiz und Systematik der herzynischen Granite. Schweizerische Mineralogische und Petrographische Mitteilungen 11–35.

Michard, G., Pearce, J. M., & Gautschi, A. (1996). Chemical evolution of waters during long term interaction with granitic rocks in northern Switzerland. *Applied Geochemistry, 11*, 757–774.

Micholet, J. (1992). Le puits de Thoune: Forage d'exploration pétrolière en Suise, Consortium Pétrolier Fribourgeois et Bernois. *Bulletin der Vereinigung schweizerischer Petroleum-Geologen und -Ingenieure, 58*, 23–32.

Mosar, J. (1999). Present-day and future tectonic underplating in the western Swiss Alps: reconciliation of basement–wrench-faulting and décollement folding of the Jura and Molasse basin in the Alpine foreland. *Earth and Planetary Science Letters, 173*, 143–155.

Müller, W. H., Naef, H., & Graf, H. R. (2002). *Geologische Entwicklung der Nordschweiz, Neotektonik und Langzeitszenarien Zürcher Weinland.* (p. 237). Nagra: Technischer Bericht 99–08.

Muralt, R., Vuataz, F., Schönborn, G., Sommaruga, A., & Jenny, J. (1997). Intégration des méthodes hydrochimiques, géologiques et géophysiques pour la prospection d'une nouvelle ressource en eau thermale. *Cas d'Yverdon-les-Bains, pied du Jura. Eclogae Geologicae Helvetiae, 90*, 179–197.

Naef, H. (2006). *Stratigraphie, Mächtigkeit und Lithofazies der mesozoischen Formationen in der Nordschweiz. Eine Kompilation von Bohrungen, Übersichts- und Aufschlussprofilen. Arbeitsbericht NAB 06-26* (71 pp). Wettingen: Nagra.

Nagra. (1985). *Sondierbohrung Böttstein. Untersuchungsbericht. Textband. Nagra Technischer Bericht NTB 85-01* (190 pp). Wettingen: Nagra.

Nagra. (1988). *Sedimentstudie - Zwischenbericht 1988. Möglichkeiten zur Endlagerung langlebiger radioaktiver Abfälle in den Sedimenten der Schweiz. Technischer Bericht 88-25* (40 pp). Wettingen: Nagra.

Nagra. (1989). *Sondierbohrung Weiach - Untersuchungsbericht. Technischer Bericht 88-08* (438 pp). Wettingen: Nagra.

Nagra. (1990). *Sondierbohrung Riniken - Untersuchungsbericht. Technischer Bericht 88-09* (125 pp). Wettingen: Nagra.

Nagra. (1991). *Sondierbohrung Leuggern. Untersuchungsbericht. Textband. Nagra Technischer Bericht NTB 88-10* (168 pp). Wettingen: Nagra.

Nagra. (2002). *Projekt Opalinuston—Synthese der geowissenschaftlichen Untersuchungsergebnisse—Entsorgungsnachweis für abgebrannte Brennelemente, verglaste hochaktive sowie langlebige mittelaktive Abfälle. Technischer Bericht 02-03* (659 pp). Wettingen: Nagra.

Nagra. (2008). *Vorschlag geologischer Standortgebiete für das SMA- und das HAA-Lager. Geologische Grundlagen. Nagra Technischer Bericht NTB 08-04* (439 pp). Wettingen: Nagra.

Oelkers, E. H., Gislason, S. R., & Matter, J. (2008). Mineral carbonation of CO_2. *Elements, 4*, 333–337.

Pearson, F. J., Balderer, W., Loosli, H. H., Lehmann, B. E., Matter, A., Peters, T., et al. (1991). *Applied isotope hydrogeology: A case study in Northern Switzerland* (p. 460). Amsterdam: Elsevier Scientific Publishers.

Peters, T., Matter, A., Meyer, J., Isenschmid, C., Ziegler, H. J. (1989). *Sondierbohrung Kaisten. Geologie, Textband Nagra Technischer Bericht NTB 86-04* (286 pp). Wettingen: Nagra.

Pfiffner, A., Erard, P.-F., & Stäuble, M. (1997). Two cross sections through the Swiss Molasse Basin (lines E4–E6, W1, W7–W10). In A. Pfiffner, P. Lehner, P. Heitzmann, S. Mueller, & A. Steck (Eds.), *Deep structure of the Swiss Alps. Results of NRP 20* (pp. 64–72). Basel: Birkhäuser.

Portier, S., & Rochelle, C. (2005). Modelling CO_2 solubility in pure water and NaCl-type waters from 0 to 300°C and from 1 to 300 bar: Application to the Utsira formation at Sleipner. *Chemical Geology, 217*, 187–199.

Ramseyer, K. (1987). Diagenese des Buntsandsteins und ihre Beziehung zur tektonischen Entwicklung der Nordschweiz. *Eclogae Geologicae Helvetiae, 80*, 383–395.

Rybach, L. (1992). Geothermal potential of the Swiss Molasse Basin. *Eclogae Geologicae Helvetiae, 85*, 733–744.

Rybach, L., Büchi, U. P., Bodmer, P., Griesser, J.-C., Israng, L., Kappeler, S., et al. (1981). *Geothermische Datensynthese der Schweiz. Schriftreihe des Bundesamtes für Energiewirtschaft, Studie Nr. 26* (p. 122). Bern: Bundesamt für Energiewirtschaft.

Rybach, L., Eugster, W., & Griesser, J.-C. (1987). Die Geothermische Verhältnisse in der Nordschweiz. *Eclogae Geologicae Helvetiae, 80*, 521–534.

Schegg, R., Cornford, C., & Leu, W. (1999). Migration and accumulation of hydrocarbons in the Swiss Molasse Basin: Implications of a 2D basin modeling study. *Marine and Petroleum Geology, 16*, 511–531.

Schegg, R., & Leu, W. (1998). Analysis of erosion events and paleogeothermal gradients in the North Alpine Foreland Basin of Switzerland. In: S. J. Düppenbecker, & J. E. Iliffe (Eds.), *Basin modelling: Practice and progress* (pp. 137–155). Geological Society Special Publication no. 141.

Schegg, R., Leu, W., Cornford, C., & Allen, P. A. (1997). New coalification profiles in the Swiss Molasse Basin: Implications for the thermal and geodynamic evolution of the Alpine Foreland. *Eclogae Geologicae Helvetiae, 90*, 79–96.

Schmassmann, H. (1990). *Hydrochemische Synthese Nordschweiz: Tertiär- und Malm-Aquifere. Nagra Technische Bericht NTB 88-07* (244 pp). Wettingen: Nagra.

Schmassmann, H., Balderer, W., Kanz, W., Pekdeger, A. (1984). *Beschaffenheit der Tiefengrundwässer in der zentralen Nordschweiz und angrenzenden Gebieten. Nagra Technischer Bericht NTB 84-21* (335 pp). Wettingen: Nagra.

Schmassmann, H., Kullin, M., Schneemann, K. (1992). *Hydrochemische Synthese Nordschweiz: Buntsandstein-, Perm-, und Kristallin-Aquifere. Nagra Technischer Bericht NTB 91-30* (493 pp). Wettingen: Nagra.

Schrader, F. (1988). Das regionale Gefüge der Drucklösungsdeformation an Geröllen im westlichen Molassebecken. *Geologische Rundschau, 77*, 347–369.

SFOE. (2007). *Energy perspectives for 2035. Management summary* (p. 20). Bern: Swiss Federal Office of Energy (SFOE).

Signer, C., & Gorin, G. E. (1995). New geological observations between the Jura and the Alps in the Geneva Area, as derived from reflection seismic data. *Eclogae Geologicae Helvetiae, 88*, 235–265.

Signorelli, S., & Kohl, T. (2006). *Geothermischer Ressourcenatlas der Nordschweiz. Gebiet des nördlichen Schweizer Mittellandes* (96 pp). Beiträge zur Geologie der Schweiz. Schweizerische Geophysikalische Kommission.

Solomon, S. (2007). *Carbon dioxide storage: Geological security and environmental issues—Case study on the Sleipner gas field in Norway* (p. 126). Oslo: Environmental Foundation Bellona.

Sommaruga, A. (1997). Geology of the Central Jura and the Molasse Basin: New Insight into an Evaporite-Based Foreland Fold and Thrust Belt. *Unpub. PhD Thesis* (176 pp). Neuchâtel: Université de Neuchâtel.

Sommaruga, A. (1999). Décollement tectonics in the Jura foreland fold and thrust belt. *Marine and Petroleum Geology, 16*, 11–134.

Sommaruga, A. & Eichenberger, U. (2010). Elevation maps and vertical thickness maps, enclosures 5 and 6. In: U. Eichenberger, A. Sommaruga, F. Marillier (Eds.), *Seismic Atlas of the Swiss Molasse Basin*. Swiss Geophysical Commission and Swiss Federal Office of Topography, Swiss Geological Survey. http:\\www.sgpk.ethz.ch.

Span, R., & Wagner, W. (1996). A new equation of state for carbon dioxide covering the fluid region from the triple-point temperature to 1100 K at pressures up to 800 MPa. *Journal of Physical & Chemical Reference Data, 25*, 1509–1596.

Thouvenot, F., Frechet, J., Tapponnier, P., Thomas, J. C., Le Brun, B., Menard, G., et al. (1998). The M-L 5.3 Epagny (French Alps) earthquake of (1996 July 15: A long-awaited event on the Vuache Fault. *Geophysical Journal International, 135*, 876–892.

Thury, M., Gautschi, A., Mazurek, M., Müller, W.H., Naef, H., Pearson, F.J., Vomvoris, S., Wilson, W. (1994). *Geology and Hydrogeology of the Crystalline Basement of Northern Switzerland. Technical Report 93-01* (400 pp). Wettingen: Nagra.

Toth, J. (1995). Hydraulic conductivity in large sedimentary basins. *Hydrogeology Journal, 3*, 4–16.

Trümpy, R. (1980). *Geology of Switzerland: a guide-book. Part A: An outline of the geology of Switzerland* (p. 104). Basel: Wepf & Co. Publishers.

US-DOE. (2008). *Carbon sequestration atlas of the United States and Canada* (2nd ed., p. 139). USA: Department of Energy.

Vollmayr, T. (1992). Strukturelle Ergebnisse der Kohlenwasserstoffexploration im Gebiet von Thun, Schweiz. *Eclogae Geologicae Helvetiae, 85*, 531–539.

Vollmayr, T., & Wendt, A. (1987). Die Erdgasbohrung Entlebuch 1, ein Tiefenaufschluss am Alpennordrand. *Bulletin der Vereinigung schweizerischer Petroleum-Geologen und -Ingenieure, 53*, 67–79.

Vuataz, F. (1982). Hydrogéologie, géochimie et géothermie des eaux thermales de Suisse et des région alpines limitrophes. *Matériaux Pour la Géologie de la Suisse, Série Hydrologie, 29*, 174.

Wildenborg, T., Holloway, S., Hendriks, C., Kreft, E., Lokhorst, A., Brook, M., Brandsma, R., Egberts, P., Larsen, M. (2005). *Building the cost curve of CO_2 storage: European sector* (162 pp). Netherlands: IEA GHG and Institute of Applied Geoscience TNO.

Xu, T. F., Apps, J. A., & Pruess, K. (2004). Numerical simulation of CO_2 disposal by mineral trapping in deep aquifers. *Applied Geochemistry, 19*, 917–936.